Lawrence Sirovich
Editor

Trends and Perspectives
in Applied Mathematics

With 78 Illustrations

Contents

Lawrence Sirovich
Division of Applied Mathematics
Brown University
Providence, RI 02912 USA
and
Rockefeller University
New York, NY 10021 USA

Editors

F. John
Courant Institute of
  Mathematical Sciences
New York University
New York, NY 10012
USA

J.E. Marsden
Department of
  Mathematics
University of California
Berkeley, CA 94720
USA

L. Sirovich
Division of
  Applied Mathematics
Brown University
Providence, RI 02912
USA

Printed on acid-free paper.

6
Singularities and Similarities in Interface Flows

Andrea L. Bertozzi, Michael P. Brenner,
Todd F. Dupont, and Leo P. Kadanoff

6.1   Introduction

The onset of singularities in systems of nonlinear partial differential equations is an important issue in fields ranging from general relativity [27], to thermodynamic phase transitions [10], to fluid dynamics [13]. The development of a mathematical singularity, when some quantity associated with the PDE "blows up," reflects the creation of a new structure in the physical system which in turn forces the mathematical formulation to change. Whether or not such singularities are possible for a given system can be a difficult question. A famous problem from the theory of homogeneous incompressible fluids is the question of finite time singularity development in the three-dimensional Navier–Stokes equation: It is unknown if an initially smooth solution can develop a finite time singularity in which the vorticity becomes unbounded [23]. To date, no rigorous proof or counterexample exists; neither numerical nor physical experiments have produced definitive answers [22, 25]. When a particular system allows finite time singularities, many related questions become relevant. For example, do all singularities have universal characteristics, or are there many possible behaviors? Which quantities are unbounded at the singular time?

In this chapter we study these questions for a model equation describing a simple hydrodynamic system that is both easily accessible to experiments and well known to develop singularities in finite time. Consider two different fluids separated by an interface that evolves with dynamics including a pressure jump determined by the Gibbs–Thomson relation

$$\Delta p = \gamma \kappa. \qquad (1.1)$$

Here, κ is the mean curvature of the surface, Δp denotes the pressure jump across the interface, and γ is the surface tension of the interface. Whenever the topology of the interface changes, the mean curvature and hence the pressure field develops a singularity. In typical situations, the singularity can also cause the flow velocity to diverge. This type of singularity happens

whenever a mass of fluid separates into two pieces. Examples in nature range from dripping faucets to nuclear fission.

The mathematical description of such surface tension driven flows includes the Navier–Stokes equation [1] for the fluid velocity $\mathbf{v}$

$$\begin{aligned} \mathbf{v}_t + (\mathbf{v} \cdot \nabla)\mathbf{v} &= -\nabla p/\rho + (\mu/\rho)\nabla^2\mathbf{v}, \\ \nabla \cdot \mathbf{v} &= 0 \end{aligned} \tag{1.2}$$

coupled with boundary conditions at the interface. Here ρ is the density, μ the viscosity, and p the pressure. At the interface we impose equation (1.1) along with the condition that the normal component of the fluid velocity is continuous across the interface and that the interface moves with the fluid velocity.

In this chapter, we consider singularity formation in a 1D model equation that follows from the above equations using the lubrication approximation and specific geometric constraints. The physical systems are flow in a Hele–Shaw cell and the flow of a thin film of viscous liquid on a solid surface. By reducing the hydrodynamic equations to a partial differential equation in only one spatial dimension we can more easily obtain numerical and analytical results.

The chapter proceeds as follows: After this section we derive the equations of motion in the two examples above. In Section 6.1.3, we present the model equation and discuss its mathematical features. In Section 6.1.4 we summarize our observations of singularity formation in the system. An important feature of the simulations is the ubiquitous presence of "similarity" (i.e., self-similar) solutions in the development of singularities. In Section 6.2, we describe in detail the types of similarity solutions associated with the model system and describe their characteristics. In Section 6.3, we present a detailed analysis of the numerically observed singularities for the model equation and demonstrate that most singularities are well described by similarity solutions. Finally, in Section 6.4 we point out unsolved problems.

6.1.1   Hele–Shaw Flow

In this case, two fluids (usually air and a viscous liquid) are trapped between two closely separated flat surfaces. For small Reynolds number, the evolution equation is the Navier–Stokes equation (1.2) without the inertial terms. The equation is simplified because the pressure is only a weak function of the z coordinate perpendicular to the flat surfaces. Thus, the essential dynamics follow from averaging the fluid velocity field over the perpendicular z direction to obtain Darcy's law [2]

$$v = -\frac{b^2}{12\mu}\nabla p(x,y). \tag{1.3}$$

in nature

flows in-

(1.2)

lensity, μ
tion (1.1)
·elocity is
the fluid

equation
·ximation
n a Hele–
l surface.
equation
rical and

:he equa-
e present
:ion 6.1.4
stem. An
of "simi-
.rities. In
ssociated
tion 6.3,
rities for
well de-
ınsolved

pped be-
nber, the
the iner-
y a weak
:hus, the
over the

(1.3)
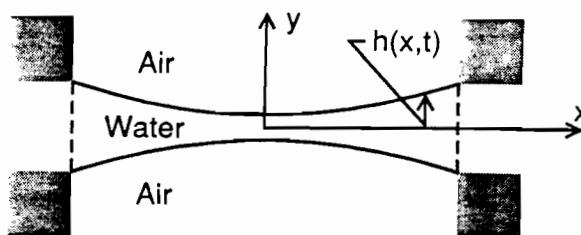
FIGURE 1.1. Picture of the thin neck in a Hele–Shaw environment. This picture is motivated by an experiment [16]. Here, $2h(x,t)$ represents the width of the neck at position x and time t.

Here b is the plate separation, μ is the viscosity, and v is the average horizontal fluid velocity. The xy plane is parallel to the flat surfaces.

We further simplify the problem by considering the evolution of a very thin neck of liquid, such as that of Figure 1.1. We assume the neck is symmetric about the center line $y = 0$ and has a small width $2h(x,t)$ which varies slowly with x. Using the lubrication approximation [7], we assume that the pressure field is independent of y, so that the x component of the velocity, u, is

$$u = -\frac{b^2}{12\mu}\partial_x p \simeq \frac{b^2\gamma}{12\mu}h_{xxx}, \qquad (1.4)$$

since in this approximation, $\kappa \simeq h_{xx}$. Finally, the conservation of mass implies that

$$h_t + l_x = 0, \qquad (1.5)$$

where $l = uh$ is the current of matter in the x direction. Combining (1.4) and (1.5) we obtain [8, 14, 15]

$$h_t + \frac{b^2\gamma}{12\mu}(hh_{xxx})_x = 0. \qquad (1.6)$$

Equation (1.6) involves two approximations: First it assumes that the Reynolds number of the flow is small. This condition might be violated near a singularity. The derivation also assumes that the width of the thin neck $2h$ is much greater than the plate spacing b. When $2h < b$, the dynamics is intrinsically three dimensional and Darcy's law (1.3) does not apply. We point out, however, that in favorable circumstances, equation (1.6) might apply until $h \sim b$. In such a situation the Reynolds number of the flow around the singularity does not become large until the flow is fully three dimensional. For more information see [4].

FIGURE 1.2. Picture of thin film of viscous liquid on a solid surface. Here, h represents the local height of the liquid at position x and time t.

6.1.2   Flow of a Thin Film

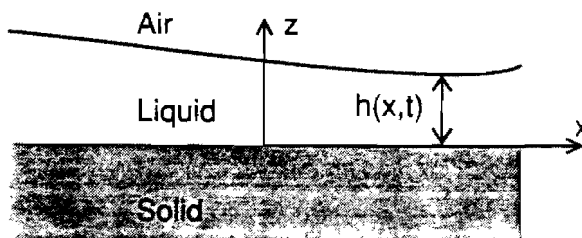In a similar fashion, we derive approximate equations for the evolution of a one-dimensional thin layer of viscous liquid on a solid surface. We consider a thin film of local thickness $h(x,t)$ (see Figure 1.2). Here, there are two different boundary conditions: the tangential component of the liquid stress tensor vanishes at $z = h(x,t)$, the air–liquid interface. In addition, we must prescribe a boundary condition at the liquid–solid interface. The classical "no-slip" boundary condition, $u_{\|}|_{z=0} = 0$ ($u_{\|}$ is the component of $\mathbf{v}$ parallel to the solid surface), is a valid approximation as long as the microscopic solid–liquid interactions do not significantly affect the macroscopic flow field [9]. This condition is reasonable for films with a thickness much larger than the range $\bar{h}$ of the solid–liquid interactions. However, the no-slip boundary condition breaks down near contact lines (where the liquid thickness approaches zero) [20, 26] and loses applicability when the film thickness is of order $\bar{h}$, a length scale that depends on the particular physical problem at hand. In all cases, the solid exerts an enormous frictional force on the liquid, so that $\partial_z u(z,t)|_{z=0}$ is very large. Thus, the boundary conditions imply that the gradient of $\partial_z u_{\|}$ is large across the liquid film, so that the dominant viscous stress in the Navier–Stokes equation is $\partial_z^2 u_{\|}$. For low Reynolds number flows, this viscous stress balances the horizontal pressure gradient, $\nabla_{\|} p$. Again using the lubrication approximation, so the pressure field is independent of the coordinate normal to the solid surface, we obtain an equation for the horizontal component of the liquid velocity

$$u_{\|} = \frac{\nabla_{\|} p(x,y)}{\mu} \left(\frac{z^2}{2} - hz - B(x,y) \right). \tag{1.7}$$

The interactions at the solid interface determine the function B. Averaging (1.7) over the z direction, we obtain

$$\bar{u}_{\|} = -\frac{\nabla_{\|} p}{3\mu} (h^2 + 3B). \tag{1.8}$$

If we assume that h is independent of y, then the equation depends on only one spatial dimension. We are interested in the case where surface tension dominates the pressure; in particular, we neglect the effect of gravity. The evolution equation for h becomes [17]

$$h_t + \left(\frac{\gamma}{3\mu}(h^3 + Bh)h_{xxx} \right)_x = 0. \qquad (1.9)$$

The choice of B depends on conditions at the solid surface. When $h \gg \tilde{h}$, we can take $B = 0$. When the surface is porous, $B = \alpha$, where α is the porosity of the surface [24]. Also of interest are polymeric liquids, which obey the boundary condition $u|_{z=0} = c\partial_z u|_{z=0}$, which yields $B = ch$. Here c is a length scale associated with the polymer [9]. The reader should note that for film thicknesses $h \ll \tilde{h}$, the term Bhh_{xxx} dominates the flux in equation (1.9).

6.1.3   The Model Equation

The examples considered above have a common feature: When h is sufficiently small, the dominant term in the flux has the same functional form, other than the exponent of h. Mathematically, these cases differ only in that the liquid velocity is proportional to h_{xxx} (Hele–Shaw and liquid on porous medium) , hh_{xxx} (polymeric liquids), and $h^2 h_{xxx}$ (macroscopic thin film). The velocities all have the general form

$$u \sim h^{n-1}h_{xxx}. \qquad (1.10)$$

In nondimensional form, neglecting the terms with higher powers of h, the evolution equation is

$$h_t + (h^n h_{xxx})_x = 0. \qquad (1.11)$$

We note that equations of this general form with $1 \le n \le 2$ also appear in the literature as slip models for modeling motion near contact lines [19, 26].

We now ask the following questions: Does equation (1.11) allow h to go to zero in finite time? Does this answer depend on on the exponent n? We will show that the value of n determines whether such singularities are possible. There are several transitions in allowable behavior as n varies, some of which are in the range corresponding to the physical models.

Mathematical Background of the Model Equation

The model equation is a fourth-order parabolic equation. The degeneracy of the equation as $h \to 0$ requires h to be bounded away from zero for standard parabolic theory to ensure well-posedness. In this work we consider equation (1.11) as an initial value problem on the bounded domain $[-1, 1]$. In general, one can use either periodic boundary conditions on the interval

or two fixed conditions for h or higher derivatives at each endpoint. We specifically consider the fixed conditions

$$h(\pm 1) = 1, \qquad\qquad h_{xx}(\pm 1) = p \qquad\qquad \text{(pressure)}, \qquad (1.12)$$

$$h(\pm 1) = 1, \qquad h_{xxx}(\pm 1) = \pm c, \quad c > 0 \qquad \text{(current)}. \qquad (1.13)$$

The boundary condition (1.12) comes from the work of Constantin et al. [8] and Dupont et al. [11] in analyzing the Hele–Shaw problem, where p has the physical interpretation of the external *pressure*. The boundary condition (1.13) corresponds a fixed *current*, drawing liquid out of the cell at a finite rate (a situation in which a singularity must occur). Another choice introduced by Bernis and Friedman [3] is

$$h_x(\pm a) = 0, \quad h_{xxx}(\pm a) = 0. \qquad (1.14)$$

In the remainder of this section we combine both theoretical results and numerical data to illustrate when singularities are allowed in (1.11). We begin with some mathematical aspects of the solutions and present rigorous results. Then, we summarize the results of numerical simulations.

Rigorous Results

Existence of Solutions

If we consider smooth initial data $h_0(x)$ satisfying the chosen boundary conditions *and* $h_0(x) > 0$, then, in general, there exists a solution to (1.11) on a finite time interval. This solution is infinitely differentiable and can be continued in time as long as $h(x, t) > 0$. The reader will find a detailed proof of this fact with the boundary conditions (1.14) in [3]. Here we summarize the main ideas as well as differences resulting from different boundary conditions. First we note that h describes a height, a non-negative quantity. Therefore, we demand that the solution satisfies $h \geq 0$ and replace (1.11) by

$$h_t + (|h|^n h_{xxx})_x = 0. \qquad (1.15)$$

Proof of local existence of solutions to (1.15) follows from first proving local existence of solutions to the regularized equation

$$h_t + (f_\epsilon(h) h_{xxx})_x = 0, \qquad (1.16)$$

where $f_\epsilon(h) \to |h|^n$ as $\epsilon \to 0$ and $f_\epsilon(h) > \epsilon$ [an example is $f_\epsilon(h) = (h^2 + \epsilon^{2/n})^{n/2}$]. For a given ϵ, the equation is uniformly parabolic and, thus, by classical theory, has a solution on a short time interval. To prove the existence of solutions to equation (1.15) we pass to the limit in ϵ. As long as $h_\epsilon(x, t)$ is bounded away from zero uniformly in ϵ, all derivatives converge uniformly to a C^∞ solution $h(x, t)$ of the original equation. If $h(x, t) > 0$, the limit is unique. Such a limiting process is crucial for proving the existence of weak solutions even when h is not bounded away from zero

[3]. We continue this process in time until $h(x,t)$ hits zero for some value of x. Notice that finite time $h \to \infty$ type singularities are impossible for many of the boundary conditions. On any finite time interval, with either the boundary conditions (1.12), (1.14), or periodic boundary conditions, $\|h_x(\cdot,t)\|_{L^2[-1,1]}$ is an a priori bounded quantity on any time interval $[0,T]$ which forbids h to become unbounded in finite time.

*for pressure b.c., can
prove
$\mathcal{E}(h) = \int \frac{1}{2}h_x^2 + ph\, dx$
dissipated
in time.

Existence and Behavior of Singularities

We ask whether it is possible for $h \to 0$ either in finite or infinite time. Clearly boundary conditions play an important role. For example, in the case of the "pressure" boundary conditions (1.12), h definitely goes to zero if $p > 2$; the issue is whether it happens in finite or infinite time (see below). Moreover, for the current boundary conditions, a finite time singularity *always* occurs; the issue is whether it occurs on the boundary or in the interior.

We begin by noting that for $n \geq 1$ if $h \to 0$, then necessarily $\int_0^{t_c} |h_{xxxx}|_{L^\infty} dt$ must blow up. We present a formal argument that can be made rigorous:

$$
\begin{aligned}
\frac{d}{dt}(h_{min}(t)) &= \frac{d}{dt}(min_x(h(x,t))) = \frac{d}{dt}(h(x_{min},t)) \\
&= h_t(x_{min},t) + h_x(x_{min},t)\dot{x}_{min} \\
&= h_t(x_{min},t) = -h^n h_{xxxx}(x_{min},t) - nh^{n-1}h_{xxx}h_x(x_{min,t}) \\
&= -h_{min}(t)^n h_{xxxx}(x_{min},t).
\end{aligned}
$$

Hence, for $n \geq 1$, $h_{min}(t)$ can only go to zero in finite time if $\int_0^{t_c} h_{xxxx}(x_{min},t)dt$, and, hence, h_{xxxx}, diverges. Here we use the fact that $h_x(x_{min},t) = 0$.

We now show a result that rules out finite time singularities for some values of n. Furthermore, we include additional results that rule out finite time singularities when h_{xx} is bounded; we observe that this bound holds in many (but not all) of our simulations. We remark that our numerical simulations indicate that the bounds on n presented here may not be sharp. See Section 6.3 for more details.

Theorem 6.1.1 *Let h be a solution to (1.11) with either periodic boundary conditions or (1.14) and smooth initial data $h_0(x) > 0$. Then (1) if $n \geq 3.5$, then there exists a unique smooth solution $h(x,t)$ for all time that satisfies $h(x,t) > 0$. (2) If $n \geq 2$, then the above is true, provided that $h_{xx}(x,t)$ remains bounded.*

The proof is an extension of the one found in [3] showing (1) to be true for $n \geq 4$. We omit some details that are identical to those found in [3]. First consider the case of periodic or (1.14) boundary conditions. We first note that $\int h_x^2$ is an energy function because integration by parts

---

(left margin notes)

ff

point. We

(1.12)

(1.13)

ntin et al.
em, where
boundary
of the cell
. Another

(1.14)

esults and
1.11). We
it rigorous
s.

boundary
1 to (1.11)
ind can be
iiled proof
ummarize
dary con-
quantity.
ice (1.11)

(1.15)

oving local

(1.16)

$) = (h^2 +$
ind, thus,
prove the
As long as
s converge
$h(x,t) >$
:oving the
from zero

yields $(d/dt) \int h_x^2 = - \int h^n h_{xxx}^2$. The Cauchy inequality then implies an a priori bound on the $C^{1/2}$ norm of h. There is also an a priori bound on $G(h, n) = \int h^{3/2-n}$ by integration by parts:

$$
\begin{aligned}
dG/dt &= (\tfrac{3}{2} - n) \int h^{\frac{1}{2}-n}(-h^n h_{xxx})_x dx \\
&= (\tfrac{3}{2} - n)(\tfrac{1}{2} - n) \int h^{-\frac{1}{2}} h_{xxx} h_x dx \\
&= -(\tfrac{3}{2} - n)(\tfrac{1}{2} - n) \left(\int h^{-\frac{1}{2}} h_{xx}^2 - \tfrac{1}{2} \int h^{-3/2} h_x^2 h_{xx} dx \right) \\
&= -(\tfrac{3}{2} - n)(\tfrac{1}{2} - n) \left(\int h^{-1/2} h_{xx}^2 - \tfrac{1}{4} \int h^{-5/2} h_x^4 dx \right).
\end{aligned}
$$

Using the fact that

$$
\left| \int h_x^4 h^{-5/2} \right| = \left| 2 \int h_x^2 h_{xx} h^{-3/2} \right| \le 2 \left[\int h^{-1/2} h_{xx}^2 \right]^{1/2} \left[\int h_x^4 h^{-5/2} \right]^{1/2},
$$

we see that for $n > 3/2$

$$
dG/dt \le 0.
$$

Hence, G is a priori bounded. For $n \ge 3.5$ this gives an a priori bound on $\int 1/h^2$ which in conjunction with the a priori bound in the $C^{1/2}$ norm of h makes it impossible for $h(x, t)$ to reach zero.

Part (2) follows similarly, by noting that for $n \ge 2$, $\int h^{-1/2}$ is a priori bounded. If h_{xx} is bounded, then $h \to 0$ implies $\int h^{-1/2}$ must become unbounded.

We now consider the constant pressure boundary conditions (1.12). In this case the energy function is $\int \varphi_x^2$, where $\varphi(x, t) = h(x, t) - h_\infty(x)$ and $h_\infty(x)$ is the minimum energy solution satisfying the boundary conditions

$$
h_\infty(x) = 1 - \frac{p}{2} + \frac{p}{2} x^2. \tag{1.17}
$$

For the linear equation, with $n = 0$, the solution tends toward h_∞ at large times. Note, however, that $h_\infty < 0$ on $(-x_{cr}, x_{cr})$, $x_{cr} = \sqrt{2/p - 1}$ for $p > 2$. For $p > 2$, the solution will not attain the "least energy" state $h_\infty(x)$ because h cannot change sign. We assume that the solution is non-negative for all time[1]; hence, we expect an alternative "least energy" state that satisfies this constraint. For $p > 2$, the correct choice is the weak solution

---

[1] $n \ge 1$ guarantees existence of a non-negative (possibly weak) solution for all time. The proof is a direct extension of a similar result described in [3].

$$w_\infty(x) = 0, \quad |x| < x_c,$$
$$w_\infty(x) = \frac{p}{2}(|x| - x_c)^2, \quad 1 \geq |x| \geq x_c, \qquad (1.18)$$
$$x_c = 1 - \sqrt{2/p}.$$

This weak solution has a jump in its second derivative at $\pm x_c$ and hence will produce a singularity in h if $h \to w_\infty(x)$ in infinite time. Thus, when $p > 2$, we always expect a singularity to form, either in finite or infinite time. The details of the infinite time case with $n = 1$ are presented in [8, 11, 28].

When $p < 2$, there need not be a singularity, since the solution can tend toward the positive solution $h_\infty(x)$. However, we cannot rigorously rule out the possibility of finite time singularities for the constant pressure boundary conditions with $n < 4$. This result follows from an extension of Theorem 1.1. First we integrate by parts to see that $\int \varphi_x^2$ is a priori bounded where $\varphi = h - h_\infty$, which, in turn, gives an a priori bound for $\int h_x^2$ and from the boundary conditions, a bound for $\int h$. A calculation shows that

$$\frac{d}{dt}\left[\int h^{2-n} + (n-2)\int h\right] = \frac{d}{dt}[H_n(h)] = -(n-2)(n-1)\int (h_{xx}^2 - ph_{xx})dx.$$

For $n \geq 2$ this time derivative is bounded from above by the constant $(n-2)(n-1)p^2/2$. Hence, finite time singularities are impossible for $n \geq 4$. Note that this bound is higher than the bound of $n \geq 3.5$ for the boundary conditions of Theorem 1.1. The boundary conditions (1.12) provide extra boundary terms that we cannot control as in the a priori estimates used for proving Theorem 1.1. However, we can show part (2) of Theorem 1.1. The bound on $\int h$ gives a bound on $\int_0^T (h_{xxx}(1) - h_{xxx}(-1))dt$ and knowing that h_{xx} is a priori bounded gives definite bounds on $\int_0^T [h_x^3(1) - h_x^3(-1)]$ and $\int_0^T [h_x(1) - h_x(-1)]$. Using these facts, we can bound all of the boundary terms in the dG/dt integral to show that G is a priori bounded on any time interval and produce the following:

Corollary 6.1.1 *Let h be a solution to (1.11) with boundary conditions (1.12) and smooth initial data $h_0(x) > 0$. If $p > 2$, then h will go to zero in either finite or infinite time. If (1) $n \geq 4$, then finite time singularities are impossible and h hits zero in infinite time. If (2) $n \geq 2$, the above is true providing that h_{xx} remains bounded.*

If we consider the "current" (1.13) boundary conditions, we force a finite time singularity to happen and the question becomes one of whether or not it happens on the boundary or in the interior. We have the following:

Theorem 6.1.2 *Let h be a solution to (1.11) with boundary conditions (1.13) and smooth initial data $h_0(x) > 0$. (1) If $n \geq 3.5$ then $h(x,t)$ goes to zero in finite time with the singularity occurring on the boundary of*

the domain, that is at least one of $h_x(1,t)$, $h_{xx}(1,t)$ $h_x(-1,t)$, $h_{xx}(-1,t)$ becomes unbounded as $t \to t_c$, and $min_I(h(x,t)) \to 0$ as $t \to t_c$ for all arbitrarily small neighborhoods I of the boundary. (2) If $n \geq 2$, then the above is true provided that on every compact set contained in the interior of $[-1,1]$ $h_{xx}(x,t)$ remains bounded.

We note that the bound on h_{xx} at the end of this theorem will depend sharply on the chosen set. Numerically we observe that the minimum of h goes to zero by moving to the boundary as it touches down for $n \gtrsim 2.0$. The proof of Theorem 1.2 follows in the same fashion as that of Theorem 1.1. We integrate by parts while keeping the boundary terms. By previous arguments, the only way that the results of Theorem 1.1 can fail is if one of the boundary terms blows up. Since h_{xxx} is constant on the boundary, at least one of $h_{xx}(\pm 1)$ or $h_x(\pm 1)$ must become unbounded. In the case where $n \gtrsim 2$, we cannot require that h_{xx} be bounded on all of I since typically its boundary value will blow up as $t \to t_c$. However, we can rule out interior singularities with the assumption that on *every* set contained in the interior of I, h_{xx} remains bounded (the bound is not uniform). The result that h goes to zero in any arbitrarily small open neighborhood of the boundary comes from the fact that one can show as in [3] that h_{xx} and h_x (and all higher derivatives) will remain bounded in a region where h remains bounded away from zero.

6.1.4   Simulations and Similarity Solutions

We summarize numerical results for the model system. Some of the results extend previous research conducted for the $n = 1$ case in [8, 11, 28]. We classify the singularities as follows:

(a) Solutions in which $h \to 0$ in finite time versus solutions in which $h \to 0$ at infinite time. In the latter situation, the infinite time singularity is a result of the solution trying to reach a "least energy" equilibrium state, $w_\infty(x)$, that has $w_\infty(x) = 0$ on a set of positive measure and a jump discontinuity in $(w_\infty)_{xx}$.

(b) Solutions which have reflection symmetry about the singular point versus solutions which do not.

(c) Solutions in which $h \to 0$ at an interior point $[x \in (-1,1)]$ versus $h \to 0$ at a boundary point $(x = \pm 1)$. Boundary singularities are necessarily asymmetric, in the sense of (b).

There are six different cases described by this list. Table 1 shows the ones we observe in our simulations. The cases listed in Table 1 are those for which we have both numerical and analytical evidence for the singularity.
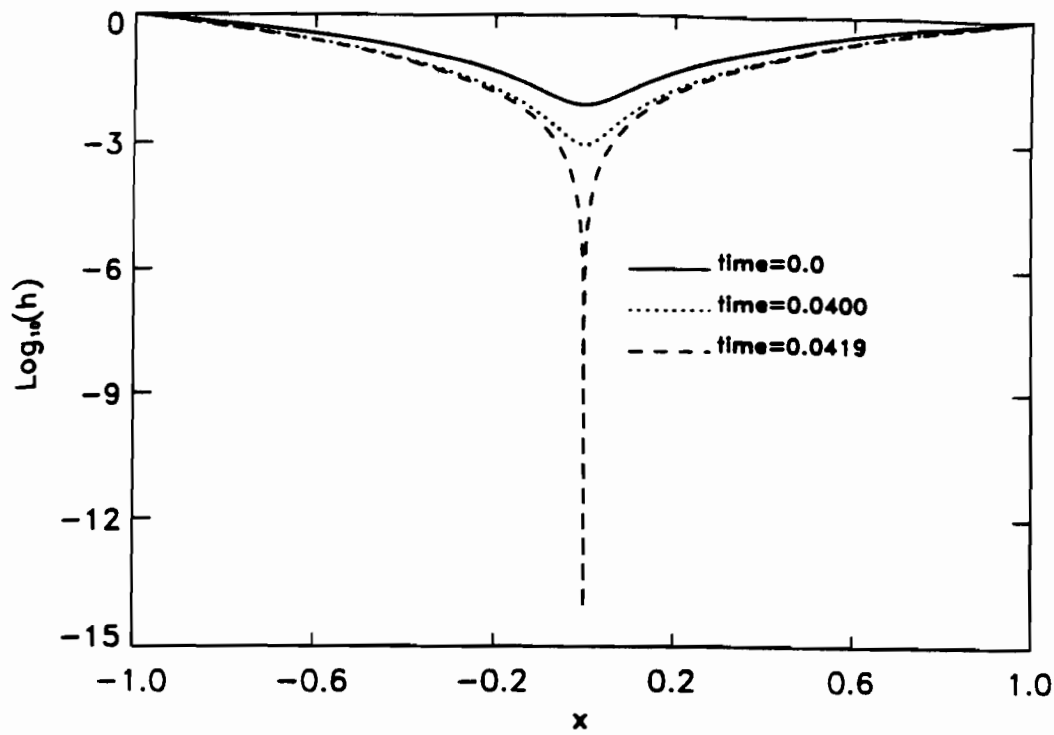
FIGURE 1.3. Finite time singularities at the center of the computational domain for $n = 0.75$. We show a log-linear plot of $h(x,t)$ for successive times before the singularity. Initial conditions and boundary conditions for this solution are detailed in Section 6.3.

(1.12)   pressure BC
(1.13)   current BC

TABLE 1. Singularities seen in simulations.

case	time	type of touchdown	boundary condition	observed for
i	finite	symmetrical	(1.12)	$0 \leq n < 1$
ii	finite	asymmetrical	(1.12) and (1.13)	$0.75 \lesssim n \lesssim 1.2$
iii	infinite	asymmetrical	(1.12)	$0.75 \lesssim n \leq \infty$
iv	infinite	symmetrical	(1.12), $p = 2$	$0.75 \lesssim n \leq \infty$
v	finite	boundary	(1.13)	$n \gtrsim 2$
vi	infinite	boundary	(1.13)	not observed

In Figures 1.3–1.6, we show typical simulation results illustrating the behaviors of Table 1. Figure 1.3 shows case (i). Here, h goes to zero at $x = 0$ ($n = 0.75$). Figure 1.4 shows case (ii). Here, h becomes small at two nonzero values of x ($n = 1.1$). Figure 1.5 shows case (v), in which a singularity occurs at the boundary of the computational domain ($n = 2.5$). Finally, Figure 1.6 shows case (iii). Here, h remains positive for all time but develops a zero at infinite time ($n = 2.0$). The zero actually develops in the entire interval $[-x_c, x_c]$. Case (iv) is a special case of (iii). Here the fact that $p = 2$ causes the singularity to be symmetric about the minimum,
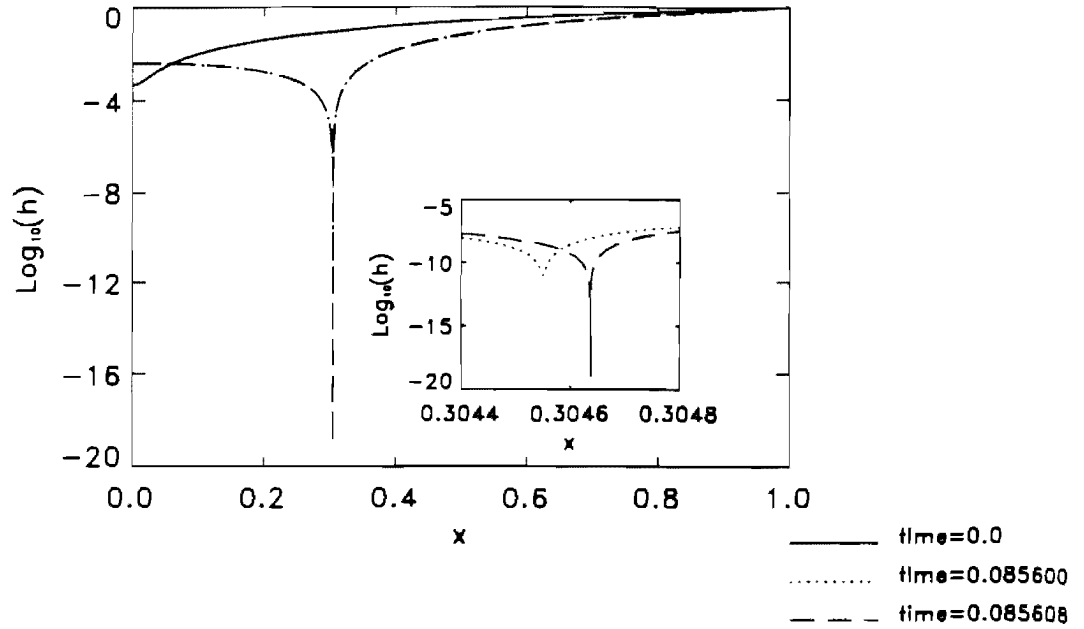
FIGURE 1.4. Finite time singularity at $\pm x_0$ for $n = 1.1$. We show a log-linear plot of $h(x,t)$ versus x for successive times before the singularity. Initial conditions and boundary conditions for this solution are detailed in Section 6.3. The inset shows a blow-up near the singularity.

since in this case $x_c = 0$.

In general, a change in the initial condition will obviously affect the nature of the solution at a later time, especially with regard to the possibility and location of singularity formation. We use the above classification because we believe that for a fixed value of n, there exists an open, possibly "large," set (in the appropriate function space) of initial conditions which lead to the same type of singularity, with many universal characteristics independent of the specific properties of the initial conditions. In our simulations, we consider a two-parameter family of initial conditions, described in Section 6.3.1. The characterizations presented in Table 1 delineate the different classes of observed singularities.

In all of the above cases, we would ideally like to *prove* that the observed behavior is possible for certain initial data and develop a detailed analytical understanding of the mathematical nature of the singularity. We lack rigorous proofs for these examples, but we can make arguments for the observed behaviors based on analytical properties of similarity solutions of the model equation. In most simulations, the region around the singularity is described by a time-independent function, apart from changes in scale;
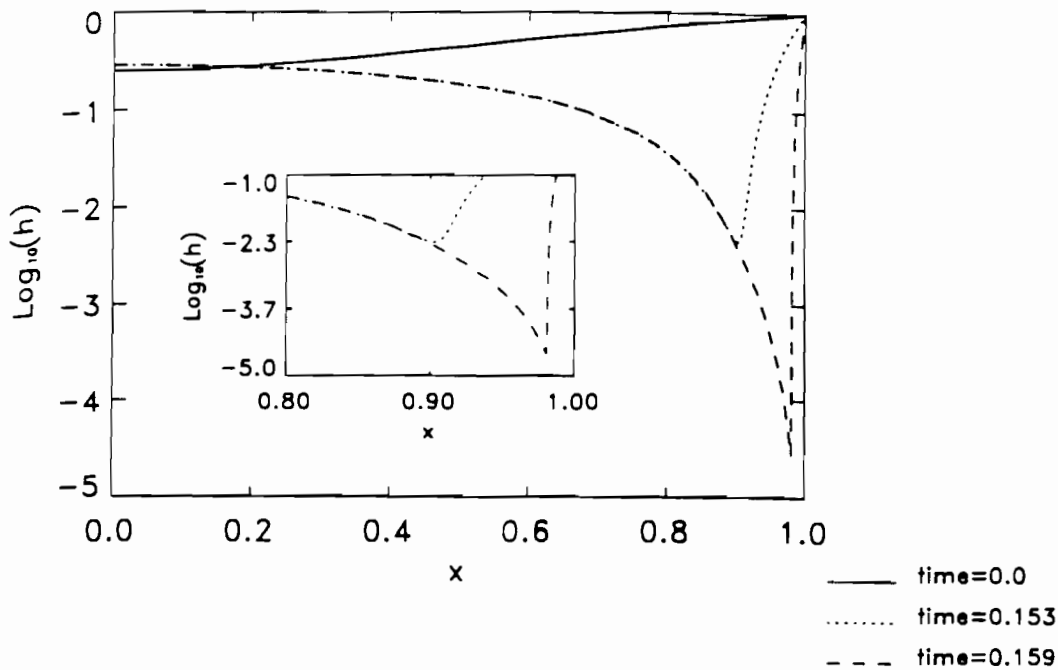
FIGURE 1.5. Finite time singularity at the edge of the simulation region for $n = 2.5$. We show a log-linear plot of $h(x, t)$ versus x for successive times before the singularity. Initial conditions and boundary conditions for this solution are detailed in Section 6.3. The inset shows a blow-up near the singularity.

that is, h has the form

$$h(x, t) = \tau(t) H(\eta), \quad \eta = \frac{x - x_p(t)}{\tau(t)^q}. \tag{1.19}$$

Here, $x_p(t)$ is the position of the minimum of h, and $\tau(t)$ is a time-dependent length scale which describes the size of the region over which the singularity occurs. A singularity happens when $\tau \to 0$. We can obtain an ODE for the shape of H by substituting (1.19) into the evolution equation and making certain assumptions about the relative size of the time-dependent terms in the equation, based on the observed behavior. We must then be able to match the similarity solution, H, at large values of η to a solution in an outer region or to boundary conditions. The matching condition puts a rather severe constraint on the types of similarity solutions that are admissible. In many of the cases described in Table 1, the matching conditions break down at specific values of n, explaining the transitions in the numerical solutions of the PDE.

In the rest of this chapter we explore the link between similarity solutions of the type (1.19) and formation of singularities in the model equation. In the next section, we discuss several classes of similarity solutions, delineated
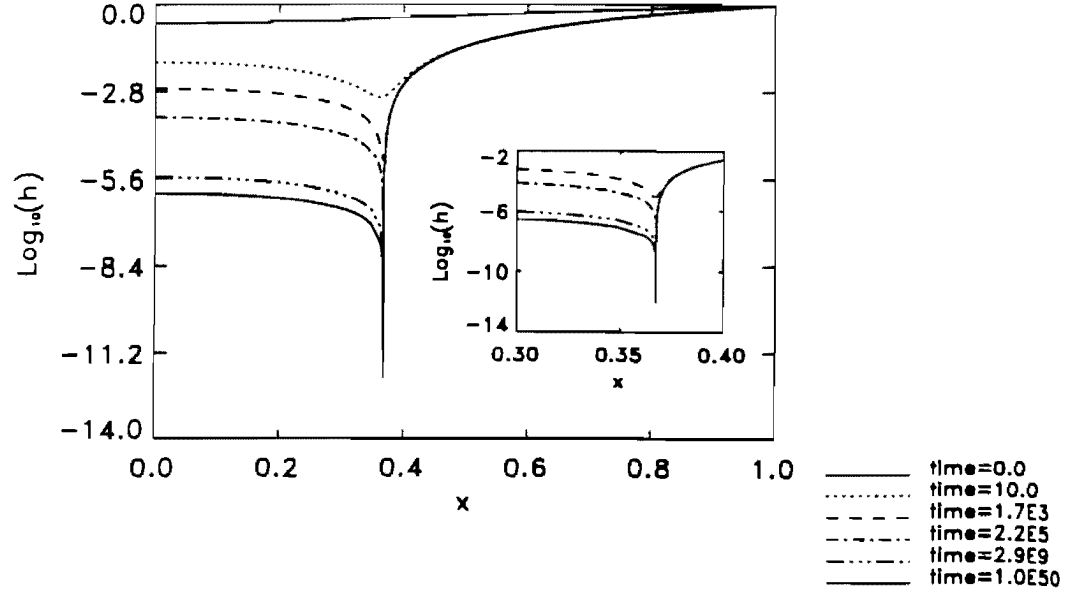
FIGURE 1.6. Infinite time singularity at $\pm x_c$ for $n = 2.0$. We show a log–linear plot of h versus x for large times. Initial conditions and boundary conditions are detailed in Section 6.3. The inset shows a blow-up near the singularity.

by the relative dominance of the different terms in the time-dependent equation. For each class, we study the admissible behavior of the functional form of H. In Section 6.3 we use the classification scheme developed in Section 2 to explain many of the observed characteristics of the numerical solutions.

6.2   The Similarity Solutions

We recall the model equation from Section 6.1,

$$h_t + (h^n h_{xxx})_x = 0. \tag{2.1}$$

We consider similarity solutions of the form

$$h(x,t) = \tau(t) H\left(\frac{x - x_p(t)}{\tau(t)^q}\right). \tag{2.2}$$

Solutions of this type arise in the numerical simulations both in the region around a singularity (the *pinch region*) and in other nonsingular parts of the solution. Typically, the scaling (2.2) represents the *dominant* behavior around a singularity; there are corrections to scaling which are of smaller order in $t_c - t$.

In order for a similarity solution to describe the region around a singularity, the solution must satisfy the following conditions:

(a) $\tau(t) \to 0$ as $t \to t_c$, the singular time.

(b) $H(\eta)$ is well behaved at large values of η, in order to match H to the outer solution or boundary conditions.

(c) $H(\eta) > 0$.

There are not always solutions which satisfy all of these conditions simultaneously. In particular, Theorem 1.1 indicates that solutions which satisfy (a) through (c) for finite t_c and $x_p \in (-1,1)$ do not exist when $n > 3.5$. In this section, we analyze the types of similarity solutions of equation (2.1) and determine the values of n for which solutions satisfying the above conditions exist.

Moreover, in our simulations, for certain boundary conditions and values of n, we observe finite time singularities which do not have the simple scaling form (2.2). By determining when a self-similar singularity is *not* possible for a system that allows for finite time singularities, we hope to gain some insight into the development of such complex singularities. We address this issue in Section 6.4.

Similarity solutions are useful for describing more than just the region around a finite time singularity. We observe self-similar solutions, typically with compact support, in other parts of the solution. Another goal of this section is to analyze the existence of these "soliton" solutions. These solutions play an important role in some of the singularity mechanisms described in Section 6.3.

6.2.1 Derivation of Similarity Solutions

Substituting the form (2.2) into the basic equation (2.1) gives

$$\frac{\tau_t}{\tau}(1 - q\eta\partial_\eta)H - \frac{\dot{x}_p}{\tau^q}H_\eta + \tau^{n-4q}(H^n H_{\eta\eta\eta})_\eta = 0. \qquad (2.3)$$

We classify self-similar solutions by assuming that, to leading order, τ and x_p have power law behavior in $t_c - t$ and then choosing relative sizes of $\dot{\tau}$, $\dot{x}_p$, and τ^{n-4q}. We emphasize that by "similarity solution" we refer merely to solutions which exhibit scaling. In some cases this scaling will yield an exact solution to (2.1). However, in most instances, the scaling gives an approximate solution that only solves (2.1) to leading order in a small variable (usually τ or a power of τ). We classify these different types of similarity solutions by the relative sizes of the time-dependent coefficients in equation (2.3).

q Equation

One possibility is that all the terms in (2.3) are of the same order of magnitude when η is of order unity. In that case, $x_p = \alpha\tau^q$, so that x_p can be

---

(left margin notes:)

time=0.0
time=10.0
time=1.7E3
time=2.2E5
time=2.9E9
time=1.0E50

a log–linear
nditions are
ty.

·dependent
functional
·veloped in
numerical

(2.1)

(2.2)

the region
ar parts of
·t behavior
of smaller

absorbed into a redefinition of the variable η.[2] The similarity equation is

$$\lambda(1 - q\eta\partial_\eta)H = (H^n H_{\eta\eta\eta})_\eta \qquad (2.4)$$

with τ given by

$$\frac{\tau_t}{\tau} = -\lambda\tau^{n-4q}. \qquad (2.5)$$

The minus sign appears because τ necessarily decreases in time. There are two unknown parameters in this equation, q which defines the scaling of the solution, and α, which determines the location of the self-similar solution in x. There are two cases: If $4q > n$, then $\tau \to 0$ in finite time, as $t \to t_c$ with the power law

$$\tau \sim (t_c - t)^{\frac{1}{4q-n}} \qquad (2.6)$$

In the other case, $4q < n$, $\tau \to 0$ in infinite time

$$\tau \sim t^{\frac{-1}{n-4q}}. \qquad (2.7)$$

Henceforth, the similarity equation (2.4) is called the q equation. So far, we have not found a situation in which the q equation describes the region around the minimum of h. However, solutions to the $q = 0$ equation do arise in the central region $[-x_c, x_c]$ for singularities of type (iii) of Table 1. Note that solutions to the q equation are exact self-similar solutions to (2.1).

Velocity Equation

Another possibility is that the motion or *velocity* of the singular point $x_p(t)$ dominates the first term in (2.3), that is,

$$|\tau^{q-1}\tau_t| \ll \left|\frac{dx_p(t)}{dt}\right|. \qquad (2.8)$$

Then assume the $\dot{x}_p(t)$ term balances the third or "current" term in (2.3) so that

$$\frac{dx_p(t)}{dt} = a\tau^{n-3q}, \qquad (2.9)$$

where a is an undetermined constant of order unity. These assumptions lead to an approximate solution to (2.3) with the self-similar form (2.2), where H satisfies

$$aH + b = H^n H_{\eta\eta\eta}. \qquad (2.10)$$

Here b is a constant of integration of order unity. Since the velocity of the minimum point, $\dot{x}_p$ dominates the time derivative of the pinch region, we call equation (2.10) the velocity equation. Notice that this solution has

---

[2]If $q = 0$, then x_p satisfies $\dot{x}_c = \tau^n$.

(2.4)

(2.5)

. There are
aling of the
lar solution
, as $t \to t_c$

(2.6)

(2.7)

ion. So far,
the region
equation do
ii) of Table
solutions to

point $x_p(t)$

(2.8)

rm in (2.3)

(2.9)

ssumptions
form (2.2),

(2.10)

ocity of the
region, we
olution has

two undefined "critical indices": We know neither the value of q nor the time dependence of τ. In general, matching conditions fixes these indices. In Section 6.3, we show that the velocity equation is relevant for understanding case (v) of Table 1, touchdown on the boundary.

Current Equation

A third possibility is that the time derivative h_t [the first two terms in (2.3)] is negligible, so that

$$\begin{aligned} |\dot{x}_p| &\ll \tau^{n-3q}, \\ |\tau_t| &\ll \tau^{n-3q}. \end{aligned} \qquad (2.11)$$

In this case, H obeys

$$(H^n H_{\eta\eta\eta})_\eta = 0. \qquad (2.12)$$

If the constant of integration, denoted by λ, is positive, we have

$$H^n H_{\eta\eta\eta} = \lambda. \qquad (2.13)$$

This equation expresses the fact that the *current* is independent of position near the singularity. Note that again the similarity solution does not fix either q, or the time dependence of τ. In Section 6.3, we show that this similarity equation applies near the singularity in several different situations, including cases (ii) and (iii) of Table 1.

Parabolic Equation

We can also consider a case where the time dependences obey (2.11) but the constant of integration in (2.13) is zero. Then, H obeys

$$H_{\eta\eta\eta} = 0. \qquad (2.14)$$

We call this the parabolic equation, for, in general, H is a quadratic function of η. In Section 6.3 we show that this solution is applicable in the central and outer regions of case (iii), and in the pinch region of case (i).

Table 2 summarizes similarity solutions we observe in the simulations. Here x_0 is the position in $[0,1]$ where the singularity occurs. Since our simulations are symmetric about 0, we see an identical singularity at $-x_0$. Section 6.3 contains detailed analysis of the connections between the simulations and the similarity solutions.

TABLE 2. Similarity solutions seen in simulations.

location of singularity	time	observed for	pinch region equation	center region equation
$x_0 = 0$	finite	$0 \leq n \leq 1$	parabolic	same
$0 < x_0 < 1$	finite	$0.75 \lesssim n \lesssim 1.2$	current	not self–similar
$0 < x_0 < 1$	infinite	$0.75 \lesssim n \leq 2$	current	q equation, $q = 0$
$0 < x_0 < 1$	infinite	$2 < n < \infty$	current	parabolic
boundary	finite	$n \gtrsim 2$	velocity	not self–similar

6.2.2 Qualitative Properties of the Similarity Solutions

First we investigate the properties of solutions relevant in the neighborhood of a singularity. These solutions must satisfy conditions (a)–(c) listed at the beginning of this section. In particular, we need to determine the values of n for which the current equation and the velocity equation admit solutions which satisfy conditions (b) and (c) above. To satisfy (b), the solution must be well behaved as $\eta \to \pm\infty$. To satisfy (c), it is necessary that the solution never crosses $H = 0$. We call the solution which satisfies both of these properties a global solution.

First we consider the current equation (2.13). As we will see in Section 6.3, this is the correct equation to describe both finite and infinite time singularities of types (ii) and (iii). We give a heuristic discussion of the types of solutions that are allowed. Reference [5] contains rigorous arguments. There are three ways in which a solution H to the current equation can behave as $|\eta| \to \infty$. The behaviors are

$$
\begin{aligned}
(L) \quad H &= A|\eta| + B|\eta|^{3-n} + \ldots, \\
(Q) \quad H &= A\eta^2 + B|\eta|^{3-2n} + \ldots, \\
(S) \quad H &= A|\eta|^{\frac{3}{n+1}},
\end{aligned}
$$

where A is positive and B and subsequent coefficients in the expansion depend on the sign of η. For the last behavior (S), A must satisfy the condition

$$
A^{n+1}\frac{3}{n+1}\left(\frac{3}{n+1}-1\right)\left(\frac{3}{n+1}-2\right) = \mathrm{sgn}(\eta). \tag{2.15}
$$

In order for solution (L) to be valid as $|\eta| \to \infty$ we need $|\eta|^{3-n} \ll |\eta|$ for large $|\eta|$, or $n > 2$. Likewise for solution (Q) to work at large $|\eta|$, we need $n > 1/2$. For solution (S) to work, A is positive; hence, (2.15) applies for $0 < n < 1/2$ or $n > 2$ if $\eta > 0$ and $n < 0$ or $1/2 < n < 2$ if $\eta < 0$.

A similar analysis holds for the compactly supported solutions. Here it is necessary to determine which solutions are possible close to the location, η_0, a zero of H; for simplicity we assume that $\eta_0 = 0$. Again there are three possible behaviors: (L), (Q), and (S), with small η expansions identical to the large $|\eta|$ expansions displayed above. Hence, for (L) to work at small $|\eta|$, we need $|\eta| \gg |\eta|^{3-n}$ or $n < 2$. Solution (Q) works if $n < 1/2$, and (S) is possible for the values of n that guarantee the positivity of A.

In Table 3 we summarize the possible behaviors of the current equation. The first two rows summarize the possible behaviors as $H \to 0$ or $H \to \infty$. The boldface symbols **L**, **Q**, and **S** denote solutions to the ODE that are parametrically stable. The last four rows summarize the possible forms of the solution. Here, a global solution is a solution that never hits zero. A soliton is a solution for which $H(\eta) = 0$ at two values of η. Other solutions satisfy $H(\eta) = 0$ at one value of η and can be continued to a positive solution either as $\eta \to +\infty$ (zero on left) or as $\eta \to -\infty$ (zero on right).

A similar analysis holds for the velocity equation (2.10). Tables 4 through 6 summarize the results of the three possible cases $b = 0$, $b < 0$, and $b > 0$.

In Table 5, we present the possible behaviors for the velocity equation with $b > 0$. In Table 6, we present the possible behavior of the velocity equation with $b < 0$.

TABLE 3. Current equation (2.13) behavior.

	$0 \leq n \leq 1/2$	$1/2 < n < 2$	$2 \leq n$
possible zeros	S $(\eta > 0)$,**L**,**Q**	S $(\eta < 0)$,**L**	**S** $(\eta > 0)$
possible infinities	**S** $(\eta > 0)$	S $(\eta < 0)$,**Q**	S $(\eta > 0)$,L,**Q**
soliton	possible	possible	not possible
global	not possible	possible	possible
zero only on left	possible	possible	possible
zero only on right	not possible	possible	not possible

TABLE 4. Velocity equation (2.10) with $b = 0$.

	$0 < n < 3/2$	$3/ < n < 3$	$3 \leq n$
possible zeros	S $(\eta > 0)$,**L**,**Q**	S $(\eta < 0)$,**L**	**S** $(\eta > 0)$
possible infinities	**S** $(\eta > 0)$	S $(\eta < 0)$,**Q**	S $(\eta > 0)$,L,**Q**
soliton	possible	possible	not possible
global	not possible	possible	possible
zero only on left	possible	possible	possible
zero only on right	not possible	possible	not possible

6.3   Simulation Results Compared with Similarity Solutions

6.3.1   Numerical Method

Our numerical scheme is an adaptation of a code described previously in [11]. Thus, some of the language here comes, with permission of the authors, from this source. The simulations use a conventional finite-difference method. The code is an implicit, two-level scheme based on central differences. We also use a dynamically adaptive mesh composed of a fixed macrogrid and adaptive microgrid for higher resolution of singularities. In certain instances, we use a multilevel microgrid for extremely fine resolution of singularities. The finite-difference scheme is essentially identical to the scheme used in [8, 11, 28]. They compared their results to simulation results obtained from a finite element method and found excellent agreement. The new features in the code are the incorporation of "current" boundary conditions (1.13), and a dynamically adaptive multilevel mesh for resolution of moving singularities.

---

ff

ns

ghborhood
sted at the
e values of
t solutions
ie solution
y that the
es both of

in Section
finite time
f the types
arguments.
iation can

expansion
satisfy the

(2.15)

$\ll |\eta|$ for
, we need
applies for

s. Here it
location,
e are three
identical to
k at small
2, and (S)

equation.
r $H \to \infty$.
E that are
e forms of
ts zero. A
r solutions
a positive
i right).

TABLE 5. Velocity equation (2.10) with $b > 0$.

	$0 < n < 1/2$	$1/2 < n < 3/2$	$3/2 < n < 2$	$2 < n < 3$	$3 \leq n$
possible zeros / possible infinities	$S(\eta > 0),L,Q$ / $S(\eta > 0)$	$L,S(\eta < 0)$ / $S(\eta > 0)$	$S(\eta < 0),L$ / $S(\eta < 0),Q$	$S(\eta < 0),L$ / $S(\eta < 0),Q$	$S(\eta > 0)$ / $S(\eta > 0),L,Q$
soliton	possible	possible	possible	possible	not possible
global	not possible	not possible	possible	possible	possible
zero only on left	possible	possible	possible	possible	possible
zero only on right	not possible	possible	possible	possible	not possible

TABLE 6. Velocity equation (2.10) with $b < 0$.

	$0 \leq n < 1/2$	$1/2 < n < 3/2$	$3/2 < n < 2$	$2 < n < 3$	$3 \leq n$
possible zeros / possible infinities	$S(\eta < 0),L,Q$ / $S(\eta > 0)$	$L,S(\eta > 0)$ / $S(\eta > 0)$	$S(\eta > 0),L$ / $S(\eta < 0),Q$	$S(\eta > 0),L$ / $S(\eta < 0),Q$	$S(\eta < 0)$ / $S(\eta > 0),L,Q$
soliton	possible	possible	possible	possible	not possible
global	not possible	not possible	possible	possible	possible
zero only on left	not possible	not possible	possible	possible	not possible
zero only on right	possible	possible	possible	possible	possible

We consider solutions to (1.11) that are symmetric about $x = 0$. Given an initial condition satisfying $h(x, 0) = h(-x, 0)$, the solution retains this symmetry. Thus, we can solve the equation on the interval $[0, 1]$, discretized by the N mesh points,

$$0 = x_1 < x_2 < \cdots < x_N = 1.$$

At each computational time, the arrays h_i and p_i, $i \in [1, ..., N]$, approximate $h(x, t)$ and $-h_{xx}(x, t)$, and v_j, $j \in [1, ..., N-1]$ approximates $h_{xxx}(x, t)$. The h_i and p_i values exist at the point x_i, and v_i is the computed third derivative at the center of the interval, $(x_i + x_{i+1})/2$. The following picture depicts these associations:

$$
\begin{array}{ccc}
x_i & v_i & x_{i+1} \\
\times & \rule{4cm}{0.4pt} & \times \\
h_i & & h_{i+1} \\
p_i & & p_{i+1}
\end{array}
$$
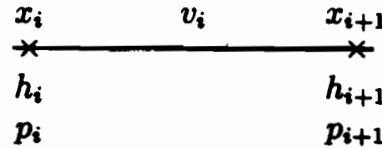
We use the notation

$$
\begin{aligned}
\Delta x_{i+1/2} &= x_{i+1} - x_i, \\
x_{i+1/2} &= \tfrac{1}{2}(x_{i+1} + x_i), \\
\Delta x_i &= x_{i+1/2} - x_{i-1/2}, \\
h_{i+1/2} &= \tfrac{1}{2}(h_{i+1} + h_i), \\
\partial h_{i+1/2} &= (h_{i+1} - h_i)/\Delta x_{i+1/2}, \\
\delta^2 h_i &= (\partial h_{i+1/2} - \partial h_{i-1/2})/\Delta x_i.
\end{aligned}
\tag{3.1}
$$

For simplicity we describe the difference scheme in space first and later indicate the time step process. We replace the equation in (1.11) by:

$$(h_i)_t + (h^n_{i+1/2} v_i - h^n_{i-1/2} v_{i-1})/\Delta x_i = 0, \tag{3.2}$$

$$v_i + \partial p_{i+1/2} = 0, \tag{3.3}$$

$$p_i + \delta^2 h_i = 0. \tag{3.4}$$

We impose the "pressure" boundary conditions by setting $h_N = 1$ and $p_N = -p$ and using the symmetry at $x = 0$. We impose the "current" boundary conditions by setting $v_N = c$, which actually fixes h_{xxx} half of a mesh point away from the boundary instead of on the boundary. This can potentially lead to numerical errors when the solution touches down on the boundary. We cut down the error by dynamically refining the mesh on the boundary as the singularity progresses. This adjustment is both effective and computationally inexpensive.

The time discretization of the above set of differential-algebraic relations uses a simple two-level scheme. In advancing from time t to time $t + dt$ we replace the time derivative terms by difference quotients involving the solution at the old time level (time t) and the as yet unknown solution at the new time level (time $t + dt$). We evaluate the other terms using a weighted average of the solution at the two time levels; a typical weight is $\theta = 0.55$ on the advanced time level and $1 - \theta = 0.45$ on the old time level.

At each time level, the fully discrete system is a set of nonlinear equations which we solve using Newton's method. If one chooses an appropriate order for the computational unknowns, the Jacobi matrix has all of its nonzero entries very close to the diagonal. Thus, the solution of the linear equations in Newton's method is not a prohibitive expense.

We dynamically choose the time steps to control several aspects of the simulation. If the result of the time step violates any of a list of constraints, it rejects the step and tries again with a smaller step size. To avoid using unnecessarily small time step sizes, if we easily meet all the constraints for several steps, we increase the step size by about 20% on the next step. The first constraint comes from local time truncation. Another constraint rejects a step for which the minimum of h decreases by more than 10%. We also assure that the correction on the first iteration of Newton's method is a very small fraction of the change over the step, where the initial guess at the change was the change over the previous step, corrected for any difference in dt's. This last constraint allows us to solve the equation using only one Newton iteration per time step.

We use highly graded spatial grids that are very fine near the singular points and less fine in other parts of the region. At any given time, the mesh has locally constant Δx_i's that increase or decrease by a factor of 2 at any point where they change. (In fact, all the Δx values are negative powers of 2.) The location of the fine grid moves as the solution evolves based on a set of rules that we vary depending on the particular simulation. For example, when we wish to resolve a finite time singularity occurring at a point $x_p(t)$ that moves with some speed (for instance, n close to 1 with current boundary conditions), we choose the degree of resolution to dynamically depend on the minimum of h and the location of the resolution to depend on the location of $x_p(t)$. When either this location moves with respect to a higher-level mesh *or* when the minimum goes beyond a certain threshold, we adapt the mesh. Regardless of the particular remeshing rule, in locations where we add mesh points, we compute h at these points by cubic spline interpolation. We compute h_{xxx} by linear interpolation between nearest neighbors. When we remove mesh points, we merely keep the values of h and h_{xxx} fixed at the remaining points. After the remeshing takes place, we decrease the time step by a factor of 20 for a single step and then resume with the former step size.

We consider a two-parameter family of "initial" conditions for both sets of boundary conditions. The parameters are chosen to be experimentally
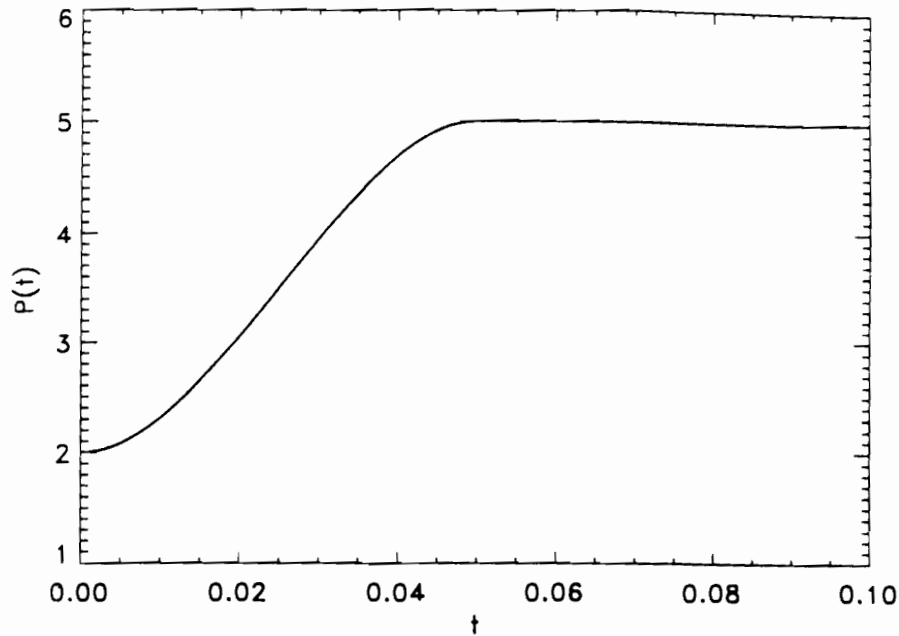
f

relations
me $t + dt$
olving the
a solution
as using a
weight is
time level.
equations
iate order
s nonzero
equations

cts of the
onstraints,
void using
onstraints
next step.
constraint
10%. We
method is
tial guess
d for any
tion using

e singular
time, the
actor of 2
negative
n evolves
mulation.
occurring
close to 1
olution to
resolution
oves with
a certain
hing rule,
se points
erpolation
erely keep
emeshing
ingle step

both sets
imentally

FIGURE 3.1. Typical profile of the boundary pressure as a function of time used in the pressure boundary conditions. We vary the value of the pressure at $t = 0$, and also the rate of increase.

realizable. In the case of the "pressure" boundary conditions, we start with a boundary pressure $p = 2 - \epsilon$, and choose the initial data to be the static parabola corresponding to this pressure

$$h(x,0) = \frac{\epsilon}{2} + \frac{(2 - \epsilon)}{2}x^2. \tag{3.5}$$

From this initial state we increase the pressure to some fixed value p. We can then consider the "initial condition" to be the state at the instant $h_{xx}(\pm 1)$ reaches its final fixed value. Figure 3.1 shows a typical graph of the boundary pressure as a function of time. We usually set the maximum p to be 5. The initial conditions thus have essentially two parameters: ϵ and the rate r at which the pressure on the boundary increases. Both of these parameters are relevant; varying either can influence the type of singularity produced.

For the current boundary conditions, we prepare the initial state by starting out with a static parabola at a pressure $p = 2 - \epsilon$ and a boundary current of zero. We then gradually increase the boundary current to its constant final value.

6.3.2 Infinite Time Singularities

Throughout this section and the rest of this chapter we use $x_p(t)$ to denote the (time-dependent) location of a minimum in h. We use x_0 [$=\lim_{t \to t_c} x_p(t)$] to denote, in general, the static location of the point where $h(x,t)$ goes to zero, and x_c denotes this location for the special case of infinite time singularities.

For $p < 2$, the constant pressure (1.12) boundary condition need not lead to a singularity. Instead, as t goes to infinity, $h(x,t)$ may approach the parabolic solution

$$h_\infty(x) = 1 - \frac{p}{2} + \frac{p}{2}x^2 \quad \text{(parabolic solution)}. \tag{3.6}$$

Expression (3.6) is the lowest-energy non-negative solution. [Recall from Section 6.1 that the "energy" for these boundary conditions is $\int \varphi_x^2 dx$, $\varphi = h(x,t) - h_\infty(x)$]. However, for $p > 2$, the parabolic solution (3.6) goes through zero. Instead, the lowest-energy function is the weak solution

$$w_\infty(x) = \begin{cases} \frac{p}{2}(|x| - x_c)^2 & \text{for } |x| > x_c \\ 0 & \text{otherwise} \end{cases} \tag{3.7}$$

with $x_c = 1 - \sqrt{2/p}$. This solution is not a classical solution to the equation as there is a discontinuity in $(w_\infty)_{xx}$ at x_c. If a finite time singularity does not intervene, the numerical solutions converge to the lowest-energy non-negative function in infinite time. When $p < 2$, h_∞ is strictly positive, so that as $h(x,t) \to h_\infty$, there is no singularity. However, if $p \geq 2$, $w_\infty(x) = 0$ for $x \in [-x_c, x_c]$, so that as $t \to \infty$ the solution must go to zero on this interval. In this particular case, we must also have a singularity in h_{xxx} since $(w_\infty)_{xx}$ has a jump discontinuity at $\pm x_c$.

We have initial conditions which lead to such infinite time singularities for all $n \gtrsim 0.75$. These initial conditions typically have $(r, \epsilon) = (100, 1)$ (see the previous section for a discussion of the two-parameter family of initial conditions), although there is some variation as a function of n. For $n < 0.75$, we have not found an initial conditions which leads to such a solution. In all cases, a finite time singularity intervenes. We conjecture that infinite time singularities exist for $n > 0.5$, although such solutions become much harder to find as $n \to 0.5$.

The infinite time singularities have the following generic structure: At large times, $h(x,t)$ develops two minima near $x = \pm x_c$. As $t \to \infty$, $h(\pm x_c, t) \to 0$ and $h_{xxx}(\pm x_c, t) \to \infty$. We call the region near $\pm x_c$ the "pinch region." The "central region" $[-x_c, x_c]$ contains a local maximum in h at $x = 0$. The height at the center (and in the entire central region) approaches zero as $t \to \infty$. The rate of decrease of the central region is slower than that in the pinch region. Finally, the outer region comprises $[x_c, 1]$ and $[-x_c, -1]$. Here, the solution approaches the static parabolas $\frac{p}{2}(|x| - x_c)^2$.

We now present self-similar solutions which accurately describe the approach to zero in the central region and the pinch region. Constantin et al. [8] carried out this analysis in great detail for the case $n = 1$; we extend their results to general n. In the central region, h approaches a similarity solution of the form $h(x,t) = h_0(t)C(x)$, where $C(\pm x_c) = 0$. There are two possible solutions of this type. The first possibility is that h is a solution to the q equation of Section 6.2. The only q equation that can describe the central region has $q = 0$, for when $q \neq 0$, the solutions do not have fixed support. The $q = 0$ solution satisfies

$$h_0(t) = \frac{\lambda}{n}t^{-1/n}$$

with

$$\lambda C = (C^n C_{xxx})_x \qquad (3.8)$$

and

$$C(\pm x_c) = 0.$$

In the language of Section 6.2, C must be a soliton solution. As shown there, this type of solution only exists for $n \leq 2$. An alternative in the central region is the parabolic solution

$$h(x,t) = h_0(t)\left(1 - \frac{x^2}{x_c^2}\right). \qquad (3.9)$$

This type of solution potentially applies to all values of n. However, it will turn out that it is only possible to match this central region solution onto the pinch region for $n > 2$. Note that the time dependence $h_0(t)$ is not fixed in this case but is determined by the matching. In both cases, $h_0(t)$ goes to zero as t goes to infinity. The solution thus asymptotically approaches the weak solution $w_\infty(x)$ in the central region.

Before proceeding to the pinch region, we check that the numerical solutions agree with the central region solutions. In Figure 3.2 we plot $h(x,t)/h(0,t)$ versus x for $n = 0.9$. We show data for five different times. The above theory predicts that the data should collapse onto a single curve. The solid line in the figure is a solution to equation (3.8) with the initial conditions $C(0) = 1$, $C_\eta(0) = 0$, $C_{\eta\eta}(0) = -2.95$, and $\lambda = 8.40$. The agreement is excellent. In Figure 3.3 we show a similar plot for $n = 3$. Again the data collapse and agree with the parabola (3.9).

Now we consider the solution in the pinch region. We focus on the pinch region near $+x_c$. (The same analysis holds near $-x_c$.) Here, we argue that h approaches a similarity solution

$$h(x,t) = h_{min}(t)H(\eta), \quad \eta = \frac{x - x_c}{\xi(t)}, \qquad (3.10)$$

where H obeys the current equation. The solution matches onto the central region as $\eta \to -\infty$ and onto the outer region as $\eta \to \infty$. The match onto
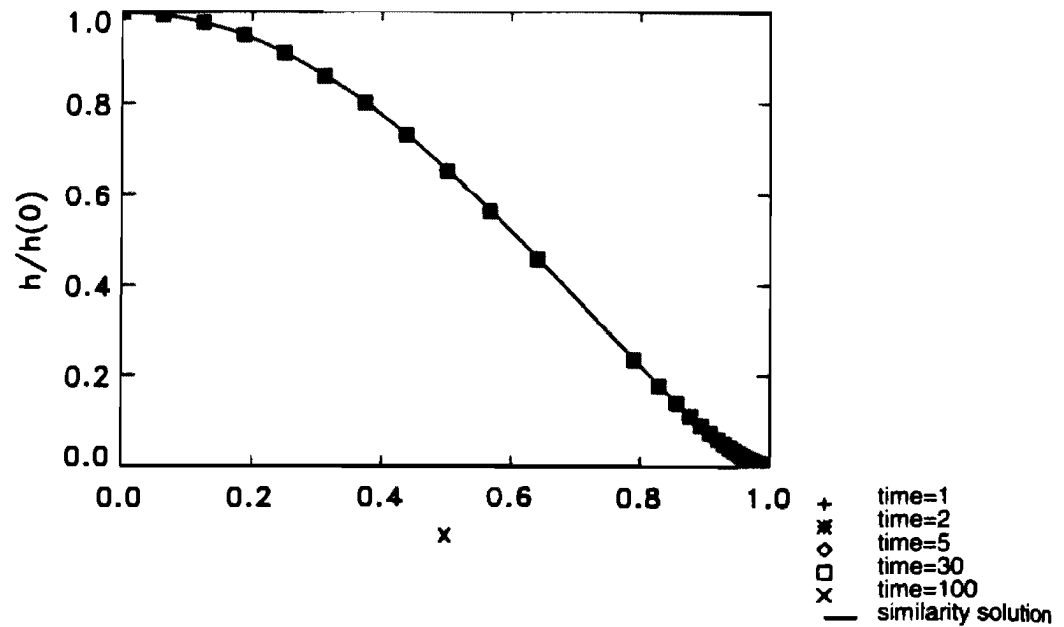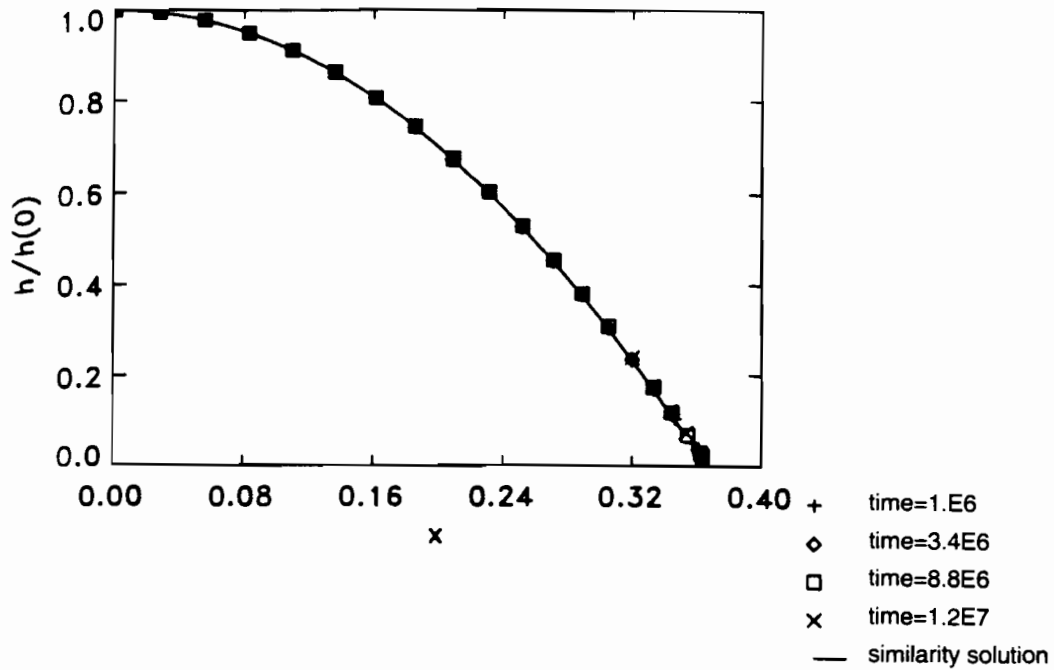
FIGURE 3.2. Rescaled profiles for the central region for $n = 0.9$. Each different symbol represents a numerical solution for a different time. The solid line is a solution to the similarity equation (3.8), computed using the conditions $C(0) = 1$, $C_\eta(0) = 0$,$C_{\eta\eta}(0) = -2.95$, $C_{\eta\eta\eta}(0) = 0$, and $\lambda = 8.40$.

the outer region requires $H(\eta) \sim A\eta^2$ at large η. The results of Section 6.2 imply this behavior is possible for $n > 1/2$ (see Table 3). Furthermore, since h_{xx} on the boundary is time independent, we need

$$h_{min} \sim \xi^2. \tag{3.11}$$

In Figure 3.4, we analyze the behavior in the pinch region by plotting $h(x,t)/h_{min}(t)$ against $(x - x_c)/h_{min}(t)^{1/2}$ for $n = 0.9$ for five different times. The similarity solution predicts that the data for different times should collapse onto a single curve. Indeed, the data collapse quite well. The solid line is a solution to the current equation with the initial conditions $H(0) = 1$, $H_\eta(0) = 0$, $H_{\eta\eta}(0) = 3.05$, and $\lambda = 1.5$.

Next, we turn to the calculation of the time-dependent coefficient $\xi(t)$ [or, alternatively, $h_{min}(t)$]. The current J from the central region, given by

$$J = \frac{d}{dt} \int_0^{x_c} h(x,t)dx,$$

fixes the time dependence of $\xi(t)$. On the other hand, the pinch region solution implies that

$$J \sim \xi^{2n-1}.$$

ʃ

+   time=1.E6
◇   time=3.4E6
□   time=8.8E6
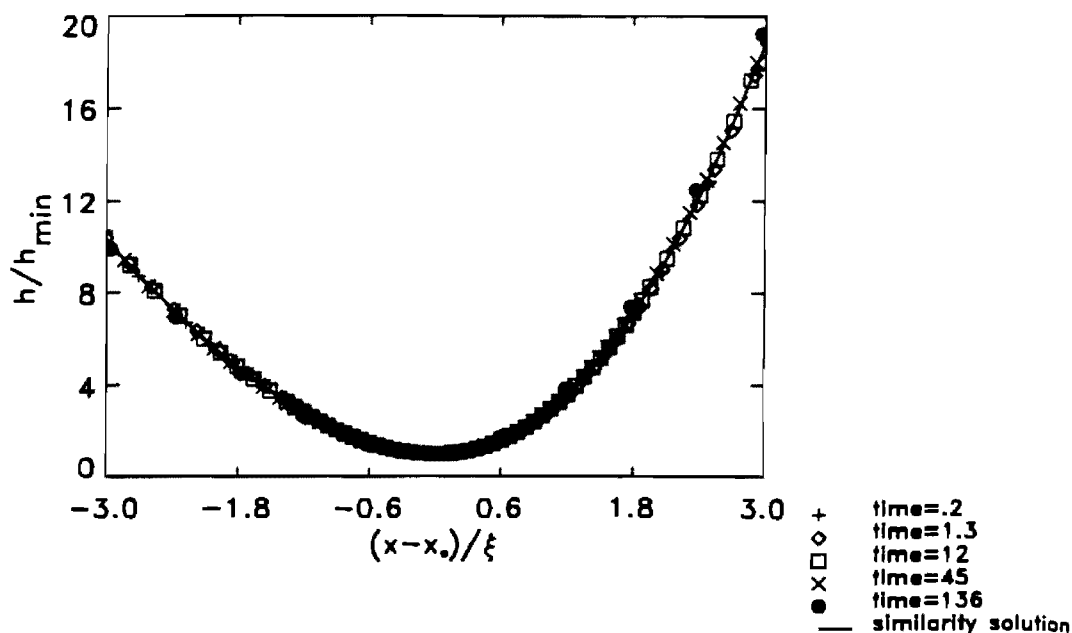×   time=1.2E7
—   similarity solution

FIGURE 3.3. Rescaled profiles for the central region for $n = 3.0$. Each different symbol represents a numerical solution for a different time. The solid line is a solution to the similarity equation (3.9).

ə=1
ə=2
ə=5
ə=30
ə=100
ilarity solution

ιch different
lid line is a
ιs $C(0) = 1$,

of Section
ιrthermore,

(3.11)

by plotting
ve different
erent times
te well. The
l conditions

ifficient $\xi(t)$
on, given by

ɔinch region

Combining these two results yields

$$h_0(t)^n \sim t\xi^{2n-1}. \tag{3.12}$$

Thus, $h_0(t)$ determines $\xi(t)$. For $1/2 < n < 2$, (3.8) gives

$$h_0 \sim t^{-1/n} \qquad (1/2 < n < 2).$$

For the parabolic solution, the time dependence is fixed by the matching: Near x_c, the edge of the central region, $h(x,t) \approx h_0(t)(x_c - x)$. This means that the solution in the pinch region must have the asymptotic behavior $H(\eta) \sim A\eta$ as $\eta \to -\infty$. From Table 3 of Section 6.2 this asymptotic behavior is only possible for $n > 2$. The match also requires the time dependences agree, so that

$$h_0(t) \sim \xi(t) \qquad (n > 2). \tag{3.13}$$

Combining these results, we find that $h_0(t)$ and $h_{min}(t)$ have the time dependences

$$h_0(t) \sim t^{-p(n)}, \quad h_{min}(t) \sim t^{-q(n)}. \tag{3.14}$$

For $1/2 < n < 2$, the exponents are

FIGURE 3.4. Rescaled profiles in the pinch region for $n = 0.9$. Each different symbol represents a numerical solution for a different time. The profiles are rescaled by $h_{min}(t)$ and $\xi(t)$, as explained in the text. The solid line is a solution to the current equation (2.13), computed using the conditions $H(0) = 1$,$H_\eta(0) = 0$, $H_{\eta\eta}(0) = 3.05$, and $\lambda = 1.5$.

$$p(n) = \frac{1}{n}, \qquad q(n) = \frac{2(1+n)}{n(2n-1)}, \tag{3.15a}$$

whereas for $n > 2$, we have

$$p(n) = \frac{1}{2(n-1)}, \qquad q(n) = \frac{1}{n-1}. \tag{3.15b}$$

Relations (3.11) and (3.15a)–(3.15b) compare very well with our numerical data. For example, in Figure 3.5 we compare log–log plots of numerical data against t for $n = 0.9$ with the slopes described by (3.15a) and find excellent agreement. In Figure 3.6 we compare log–log plots for numerical data against t for $n = 3.0$ with the slopes described in (3.15b), again with excellent agreement.

We perform similar analyses for many values of n. As a summary of these results in Figure 3.7 we show our empirically determined values of $p(n)$ (from least squares fit on the data) plotted against theoretical values for a wide range of n. In Figure 3.8 we show a similar plot for $q(n)$. No discrepancies seem to exist.
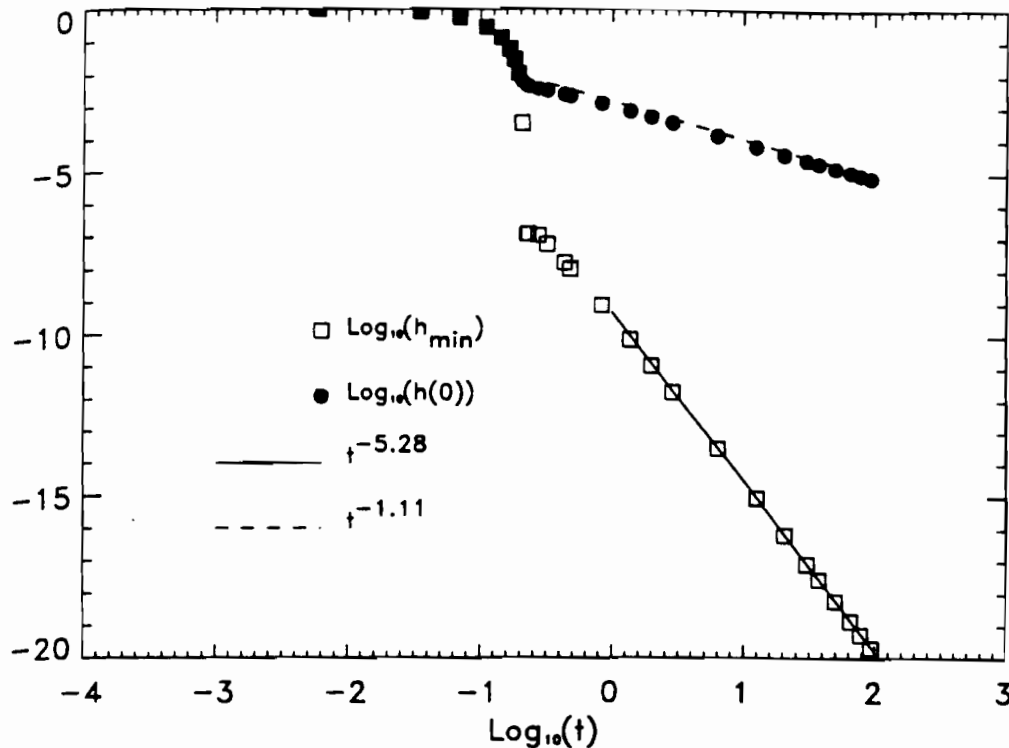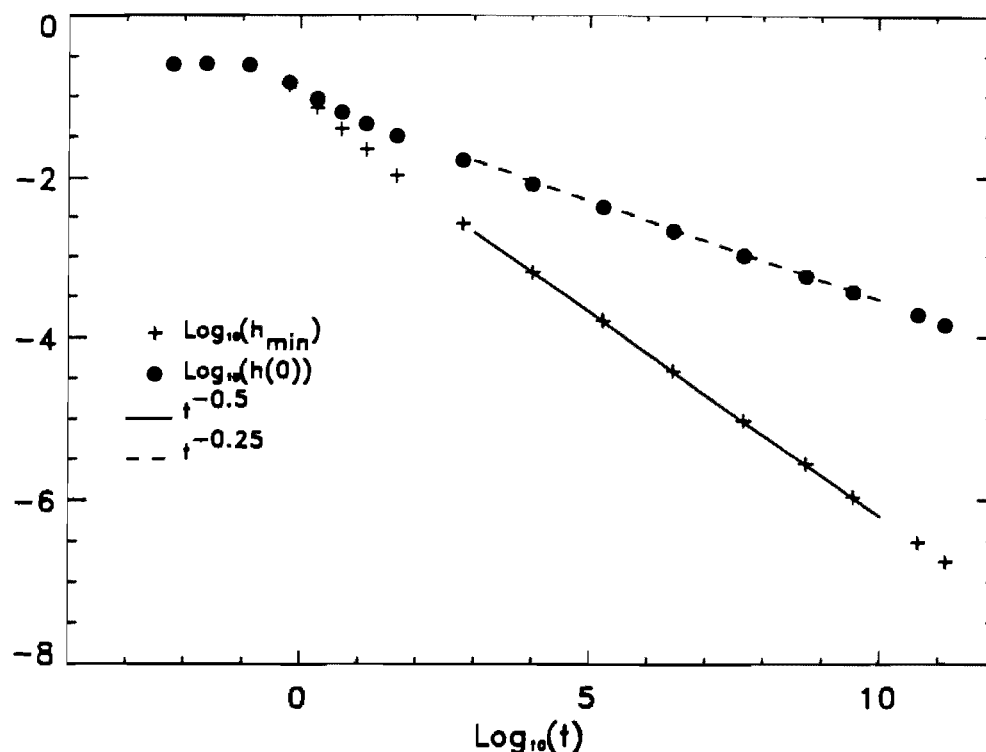
FIGURE 3.5. Time dependences of the minimum height, h_{min}, and the height $h(0,t)$ for $n = 0.9$. The solid and dashed lines are the predictions of the theory.

6.3.3 Finite Time Singularities at $\pm x_0$, $0 < |x_0| < 1$

The analysis of the preceding section is simplified by the fact that the singular point does not propagate. In this section we describe a *finite time* singularity in which the singular point does propagate. Dupont et al. [11] and Zhou [28] first discovered and analyzed this singularity in the case $n = 1$, using initial data with $(r, \epsilon) \approx (100, 1/64)$.

The singularity has the same overall structure as the previous infinite time case: There is a pinch region, a central region and an outer region. As before, we model the solution in the pinch region by a similarity solution of the form

$$h(x,t) \approx h_{min}(t)H(\eta), \quad \eta = \frac{x - x_p(t)}{\xi(t)}, \tag{3.16}$$

where H obeys the current equation with current

$$J(t) = \frac{h_{min}(t)^{n+1}}{\xi(t)^3} \tag{3.17}$$

and the pinch point $x_p(t)$ is a linear function of time as $t \to t_c$. However, in contrast to the infinite time singularities, the central region and outer

FIGURE 3.6. Time dependences of the minimum height, h_{min}, and the height $h(0,t)$ at $x = 0$ for $n = 3.0$. The solid and dashed lines show the predictions of the theory.

regions do not converge as $t \to t_c$ to simple similarity solutions. Hence, the matching of the pinch region to the rest of the solution is more complicated than in the previous case. In this section we focus only on the leading order behavior (3.16) in the pinch region.

We have numerical evidence for this finite time singularity for $0.75 \lesssim n \lesssim 1.25$ with both pressure and current boundary conditions.[3] The outer region is roughly parabolic. This suggests the pinch region scaling

$$h_{min}(t) \sim \xi(t)^2,$$

and, moreover, as $\eta \to \infty$,

$$H(\eta) \sim c\eta^2. \tag{3.18}$$

Table 3 of Section 6.2 states that this asymptotic behavior is only possible for $n > 1/2$. To illustrate the characteristics of this type of singularity we

---

[3]It is more difficult to find initial conditions which access this solution with the pressure boundary conditions. Here, we only find this type of singularity for $0.80 < n < 1.20$.
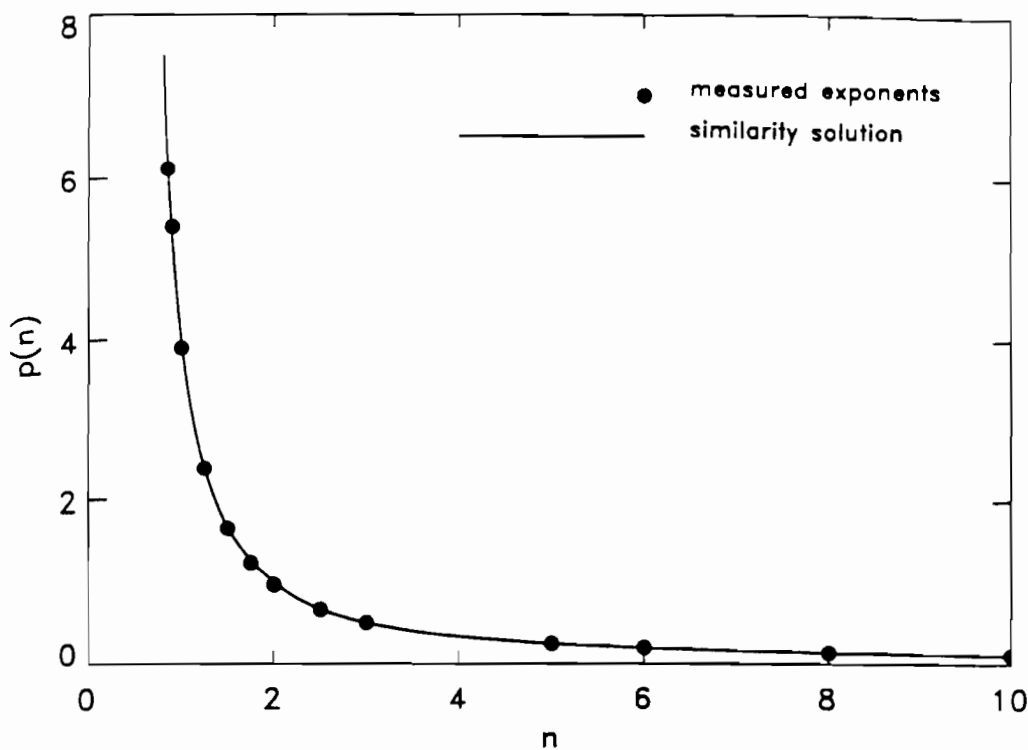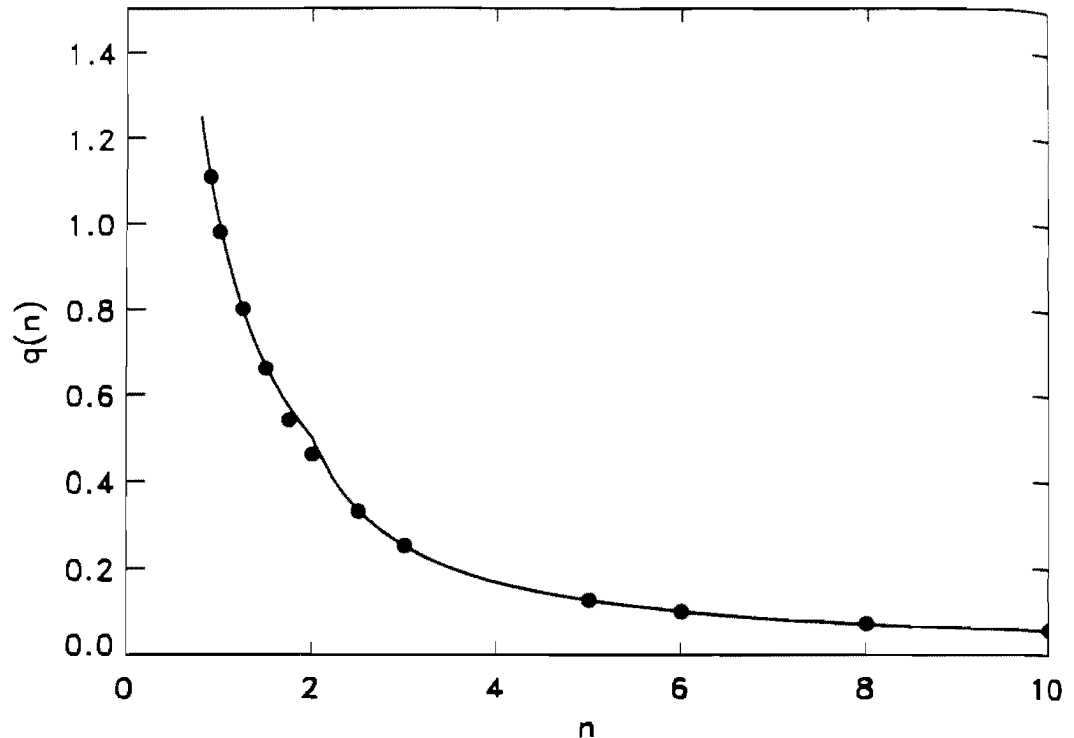
FIGURE 3.7. Exponent $p(n)$ of $h_{min} \sim t^{-p(n)}$ as a function of n. The measured exponents are compared with those of the similarity solution, equations (3.15a) and (3.15b). Error bars, as determined by the least squares fit, are typically ± 0.01. There is also a significant error which depends on the rate of convergence of the similarity solution.

show numerical results for the case $n = 1.1$. Figure 3.9 shows $h_{min}(t)$ as a function of $t_c - t$ and indicates that the singularity occurs in finite time. To illustrate that the pinch region obeys (3.18), in Figure 3.10 we show a plot of h_{xx} versus x at several different times close to the singular time for $n = 1.1$. Indeed, on the edges of the pinch region, h_{xx} approaches a constant value. Figure 3.11 shows a plot of $h(x,t)/h_{min}(t)$ as a function of $(x - x_p(t))/h_{min}^{1/2}$ for five different times, where we numerically compute $x_p(t)$ to satisfy $h(x_p(t), t) = h_{min}(t)$. The collapse of the data verifies the self-similar behavior of the solution. The solid line is a solution to the current equation with $H(0) = 1$, $H_\eta(0) = 0$, $H_{\eta\eta}(0) = 1.7$, and $\lambda = 0.5$. The agreement is excellent. We see roughly the same scaling behavior for solutions with $1.25 \gtrsim n \gtrsim 0.75$.

In order to completely understand this singularity we need to determine $h_{min}(t)$. This requires a complete match to the outer and central region. Dupont et al. [11] accomplished this for the $n = 1$ case. The corrections

d the height
redictions of

Hence, the
omplicated
ıding order

).75 $\lesssim n \lesssim$
ıe outer re-
g

(3.18)

ıly possible
gularity we

ɔlution with
ıgularity for

FIGURE 3.8. Exponent $q(n)$ of $h(0) \sim t^{-q(n)}$ as a function of n. The measured exponents are compared with those of the similarity solution, equations (3.15a) and (3.15b).

involve logarithmic terms and predict that for $n = 1$,

$$J(t) \sim (t_c - t)/|\ln(t_c - t)|. \tag{3.19}$$

This agrees quite well with the $n = 1$ numerical data. However, we do not know how to extend the result (3.19) beyond the special case $n = 1$. So far, we do not find completely convincing results from either the numerics or the analytics.

6.3.4 Edge Singularities

For large values of n, finite time singularities do not occur in the interior of the spatial domain.[4] However, one can force a finite time singularity at any value of n by using the current boundary conditions (1.13) which specify the constant rate at which $\int h$ decreases. In this specific case, h

---

[4]This fact is forced upon us for $n > 3.5$ by the theorems of Section 6.1 (see, in particular, Theorem 1.2 of Section 6.1).
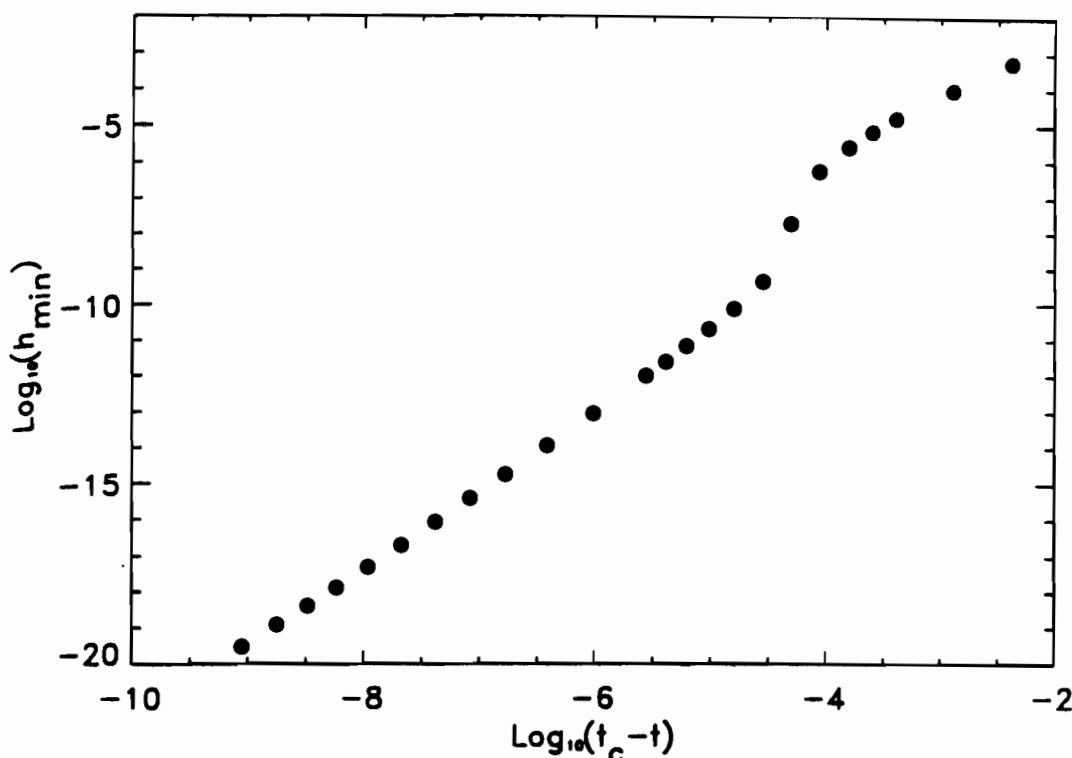
FIGURE 3.9. Time dependence of asymmetrical finite time singularities for $n = 1.1$. We show $\log(h_{min})$ versus $\log(t_c - t)$.

must go to zero in finite time, causing a singularity. For large n, the system forms singularities at the edge of the domain ($x = \pm 1$), as in the case of Figure 1.5. In our simulations, we observe that singularities form on the edge of the computational domain for $n > 2$. For $n < 1.5$, we never observe such an edge singularity. Our simulations are inconclusive as to whether the singularity forms in the interior or the edge for $1.5 < n < 2$.

The $n > 2$ edge singularities have a characteristic form. The minima of h, at $\pm x_p(t)$, progress to the boundary. For simplicity, we again consider the side close to the $x = 1$ boundary. Near the boundary but far from $x_p(t)$, $h(x,t)$ is a parabola:

$$h(x,t) = \frac{(x - x_p(t))^2}{(1 - x_p(t))^2} \quad \text{for} \quad 0 < \frac{x - x_p(t)}{1 - x_p(t)} \sim 1. \qquad (3.20)$$

The current in the pinch [near $x_p(t)$] is quite small, and in fact goes to zero as $t \to t_c$. Hence, the current at the boundary, which is fixed by the boundary condition, controls the flow out of the region $[x_p, 1]$. For $t < t_c$,
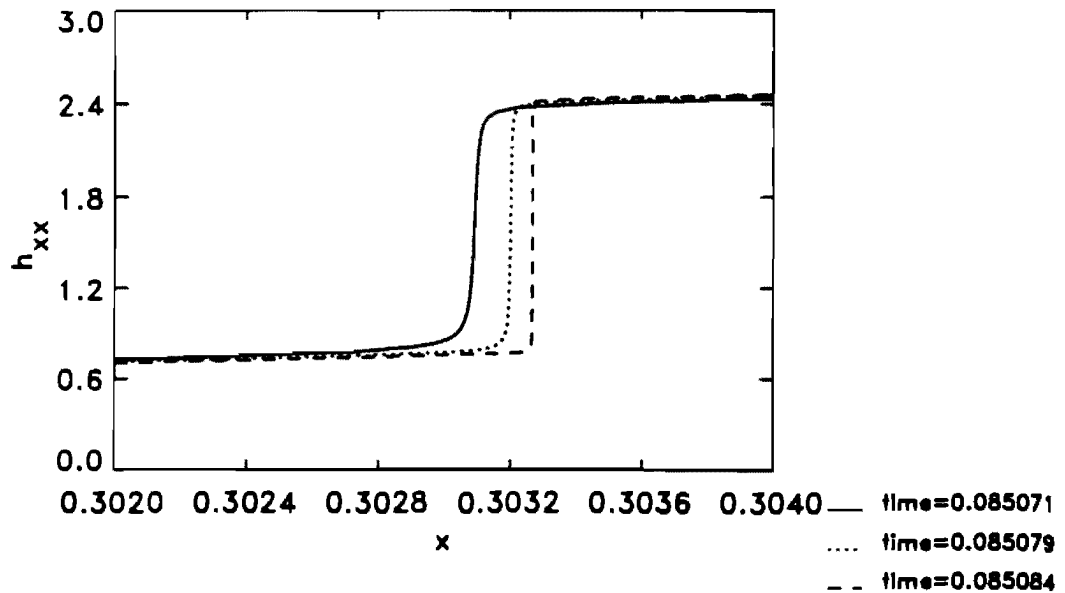
FIGURE 3.10. Plot of h_{xx} versus x in the region around the singularity near the singular time for $n = 1.1$.

the constant current boundary condition fixes the time derivative of x_p as

$$J(x = 1, t) \approx -\partial_t \int_{x_p}^{1} h(x, t) \sim \frac{dx_p(t)}{dt}, \qquad (3.21)$$

using equation (3.20). Since $J(1, t) \sim 1$ we find $x_p(t) \sim 1 - c(t_c - t)$.

In the pinch region, h is described by a similarity solution

$$h(x, t) = \xi^s H(\eta), \quad \eta = \frac{x - x_p(t)}{\xi(t)}. \qquad (3.22)$$

Here, s is an as yet undetermined parameter. Since the time derivative of ξ^s is small compared with the change in $h(x, t)$ due to the propagation of the singular point, H obeys the velocity equation of Section 6.2 and hence satisfies

$$aH + b = H^n H_{\eta\eta}. \qquad (3.23)$$

Also ξ satisfies

$$\xi^{sn-3} \sim \frac{dx_p(t)}{dt} \sim \text{constant} \qquad (3.24)$$

so that $s = 3/n$. In order for H to fit onto the quadratic form (3.20), we need both $H(\eta) \sim \eta^2$ as $\eta \to \infty$, and that ξ^{sn-2} be proportional to $(1 - x_p(t))^{-2}$. We thus find the time dependence

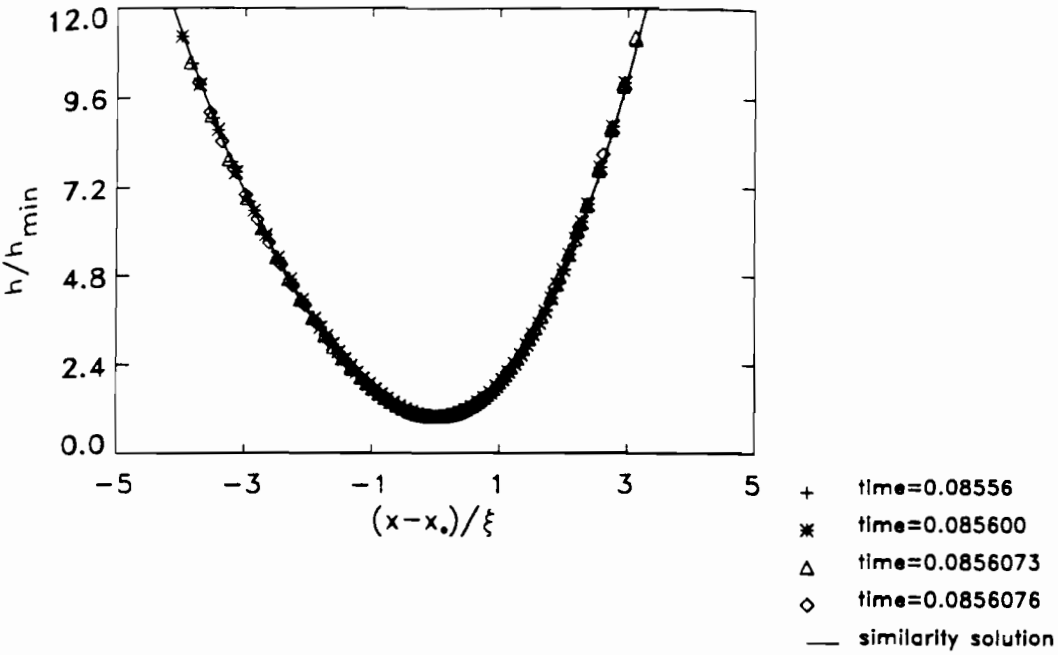$$\xi(t) \sim (t_c - t)^{2n/(2n-3)}. \qquad (3.25)$$

FIGURE 3.11. Rescaled profiles for the pinch region for $n = 1.1$. Each symbol represents a numerical solution at a different time. The solid line is a solution to the current equation, with $H(0) = 1$, $H_\eta(0) = 0$, and $H_{\eta\eta}(0) = 1.70$. The parameter $\lambda = 0.5$.

The matching to the outer region breaks down for $n < 3/2$, since equation (3.23) does not admit the asymptotic behavior $H \sim A\eta^2$ in this regime. This similarity solution can only describe singularity formation on the boundary for $n > 3/2$.

In order to complete the solution we must match to the central region. Recall in the case of infinite time singularities, the flux or current of fluid leaving the central region determines time dependences in the pinch region. Here the time dependence (3.25) follows from only the match to the boundary conditions. However, it is still true that the flux of fluid from the central region affects the solution. The neglect of this flux is only valid near the boundary, where the total flux is of order one [much larger than the flux from the central region, which is $O(\xi^s)$].

We verify that near the boundary, the similarity solution (3.23)–(3.24) holds. To check this we look at the specific case $n = 7.5$. We study the solution near $x^*(t)$, the maximum of h_{xxx}. The maximum x^* occurs to the right of x_p, the minimum of h. As $t \to t_c$, $h_{xxx}(x^*(t), t)$ diverges. Figure 3.12 shows the relation between $h_{xxx}(x^*(t), t)$ and $\xi(t)$. Figure 3.13 shows the dependence of $x^*(t)$ on $t_c - t$. Figure 3.14 shows the dependence of $h_{xxx}(x^*(t), t)$ on $t_c - t$. The solid line in each case shows the prediction of the similarity solution. The agreement is excellent. We also need to check
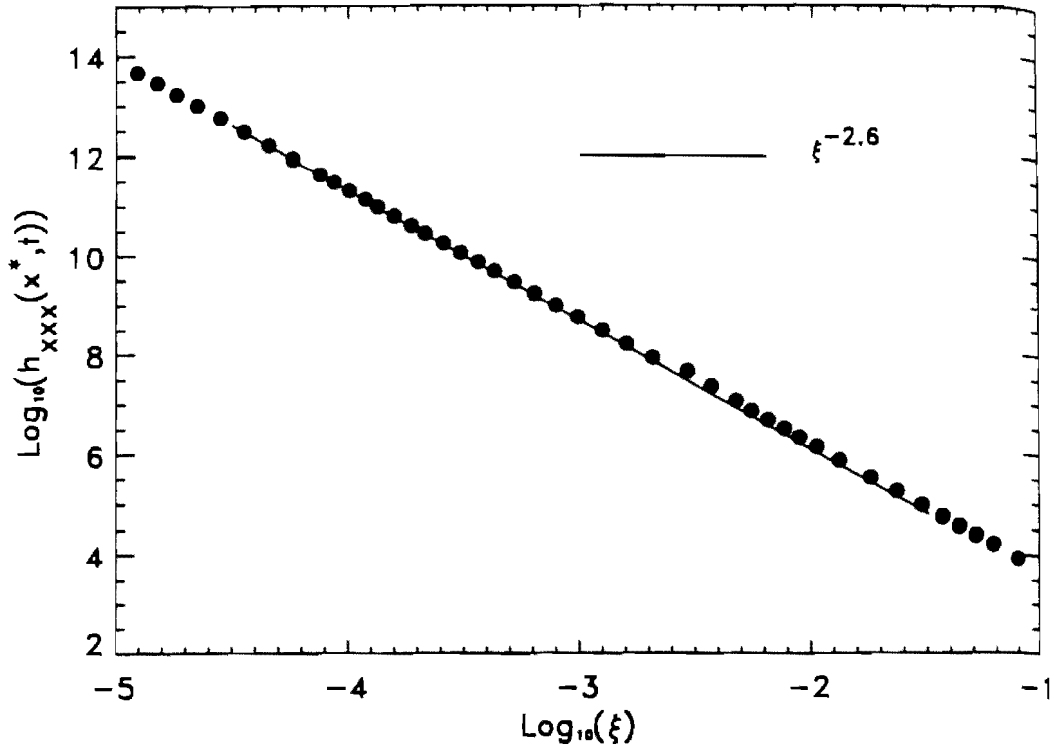
FIGURE 3.12. Dependence of $h_{xxx}(x^*, t)$ on ξ in for touchdown on the boundary, $n = 7.5$. The solid line represents the prediction of the theory.

that the functional form around the minimum is described by a solution to equation (3.23). It is *not* possible to fit the data with a single solution to the velocity equation. Upon rescaling, equation (3.23) becomes

$$H_{\eta\eta\eta} = c\frac{\text{sgn}(b) + \text{sgn}(a)H}{H^n} \tag{3.26}$$

where $\text{sgn}(a)$ denotes the sign of a. For simplicity we take $\eta = 0$ to correspond to x^*. The sign of a is necessarily positive since from above $\text{sgn}(a) = \text{sgn}(\dot{x}_p)$. The fact that $x^* \neq x_p$ in the simulations means that $\text{sgn}(b) = -\text{sgn}(a)$. It follows from this that $(H_{\eta\eta\eta})_\eta = 0$ both at the maximum of $H_{\eta\eta\eta}$ and the minimum of H. Although $(H_{\eta\eta\eta})_{\eta\eta} < 0$ at the maximum of $H_{\eta\eta\eta}$, $(H_{\eta\eta\eta})_{\eta\eta} > 0$ at the minimum of H, indicating that the similarity solution veers from the data at the minimum of H. This disagreement is a natural consequence of neglecting of the flux from the central region. As emphasized above we do not expect the similarity solution to hold for $x < x_p$.

However, a solution of (3.26) fits the data up to the minimum of h. This solution satisfies the conditions $H_{\eta\eta\eta}(0) = 1$ (an arbitrary choice) and also $H(\eta) \to 1$ as $\eta \to -\infty$. These two boundary conditions *completely*
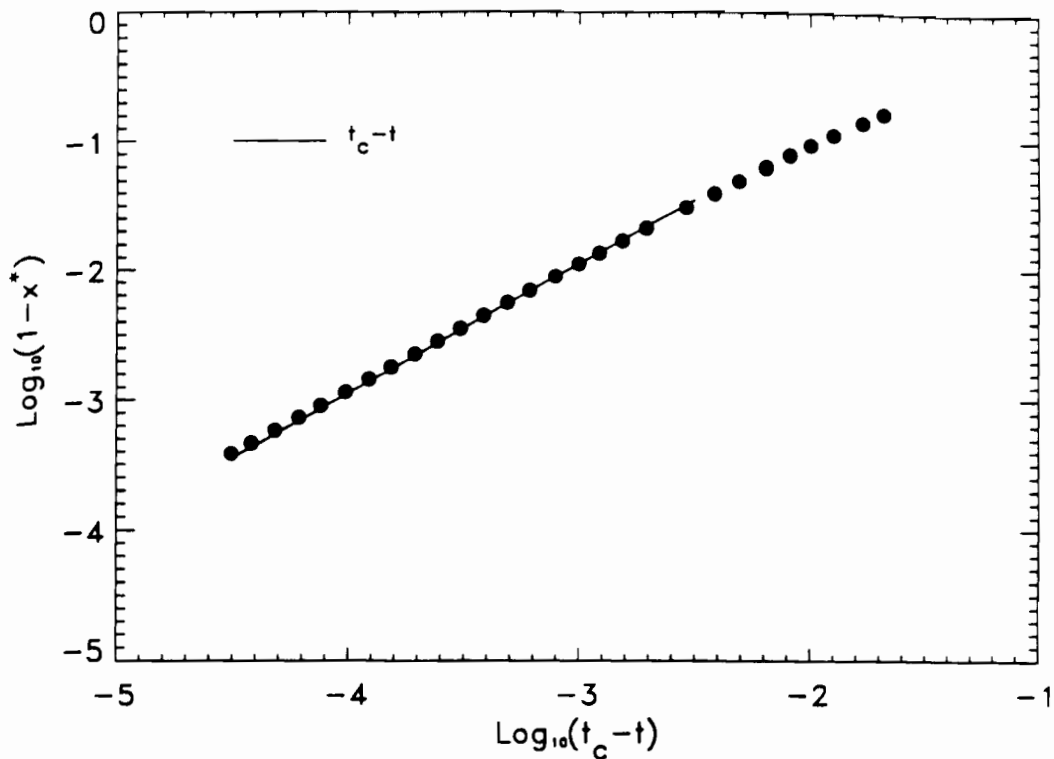
FIGURE 3.13. Dependence of $x^*(t)$ on $t_c - t$ for touchdown on the boundary, $n = 7.5$. The solid line gives the prediction of the theory.

determine the solution, for there are two exponentially growing solutions of the linearized (3.26) as $\eta \to -\infty$. The solution satisfying these conditions for $n = 7.5$ has $H(0) = 7.5/6.5$, $H_\eta(0) = 0.3542$, and $H_{\eta\eta}(0) = 0.7077$. In Figure 3.15 we compare this solution with results of a numerical simulation. In the upper half of the figure we show $h(x,t)/h_{xxx}(x^*(t))^{-1/6.5}$ versus $(x - x^*(t))/h_{xxx}(x^*(t))^{-7.5/19.5}$ for four different times. In the lower half of the figure we show $h_{xxx}(x,t)/h_{xxx}(x^*(t))$ versus $(x - x^*)/h_{xxx}(x^*(t))^{-7.5/19.5}$. The solid lines are the solutions described above. Indeed, the agreement between the similarity solution and the data is excellent up to the minimum of h, where the numerical data clearly deviate from the similarity solution. Beyond this point, the numerical data do not even collapse. Furthermore, there is an interesting dynamic structure in this region (not visible in Figure 3.15) that we defer until Section 6.4.

The similarity solution seems to agree with the numerics for a wide range of n. As an indication, in Figure 3.16 we show the scaling exponent $q(n)$ of $h_{xxx}(x^*, t) \sim \xi^{q(n)}$ as a function of n. In Figure 3.17 we show the scaling exponent $p(n)$ of $h_{xxx}(x^*, t) \sim (t_c - t)^{p(n)}$. The points represent the result of least squares fits to the data. The error in the points depends on how close the simulation is to t_c, the singular time. In each case, the solid line
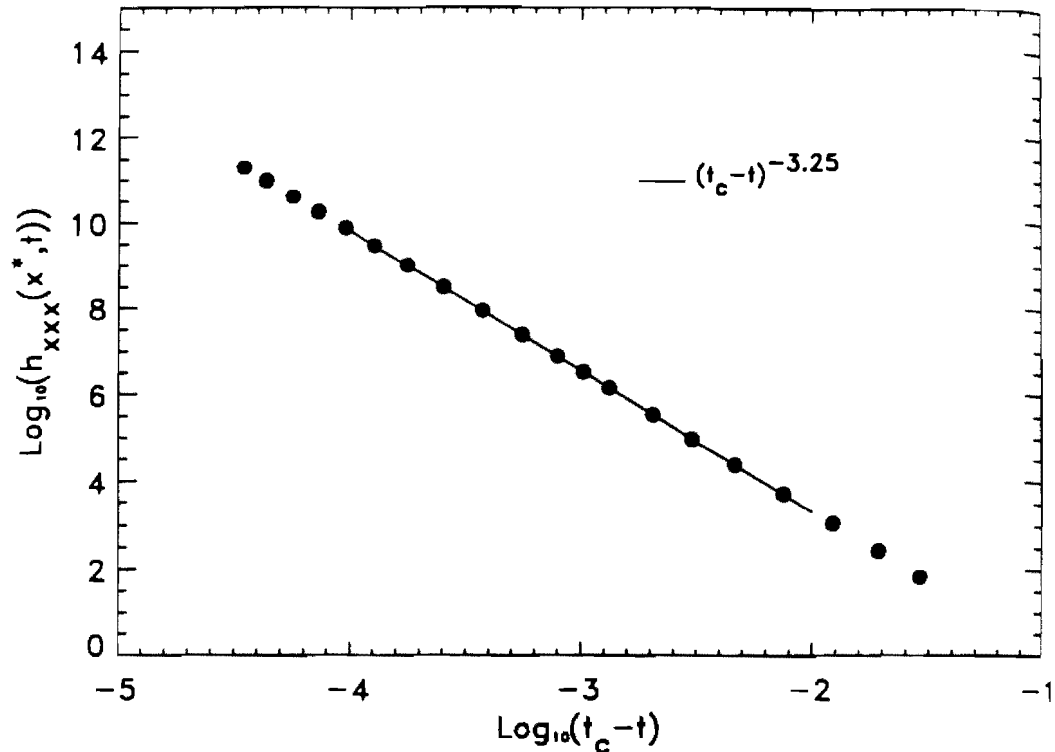
FIGURE 3.14. Dependence of $h_{xxx}(x^*, t)$ on $t_c - t$ for touchdown on the boundary with $n = 7.5$. The solid line shows the prediction of the theory.

represents the prediction of the similarity solution

$$p(n) = \frac{6(1-n)}{2n-3}, \qquad q(n) = \frac{3}{n} - 3. \qquad (3.27)$$

The agreement is quite reasonable. However, we caution that Figures 3.16 and 3.17 do *not* indicate that the similarity solution describes the data down to $n = 1.5$. Without a match to the central region we cannot accurately predict the range of n over which the solution is valid. Recall that in the previous sections the crucial factor in determining when a similarity solution breaks down is the matching to the other regions. In Section 6.4 we present some interesting features of the matching region, illustrating its nontrivial nature.

6.3.5   Finite Time Singularities at $x_0 = 0$

All of the finite time singularity mechanisms so far considered have pinch regions which are asymmetric under reflection about $x_p(t)$. We also observe

-1

;he boundary

(3.27)

Figures 3.16
es the data
annot accu-
Recall that
a similarity
Section 6.4
ustrating its

l have pinch
also observe

+   time=0.1112
*   time=0.1123
△   time=0.11260
◇   time=0.112604
—   similarity solution

+   time=0.1112
*   time=0.1123
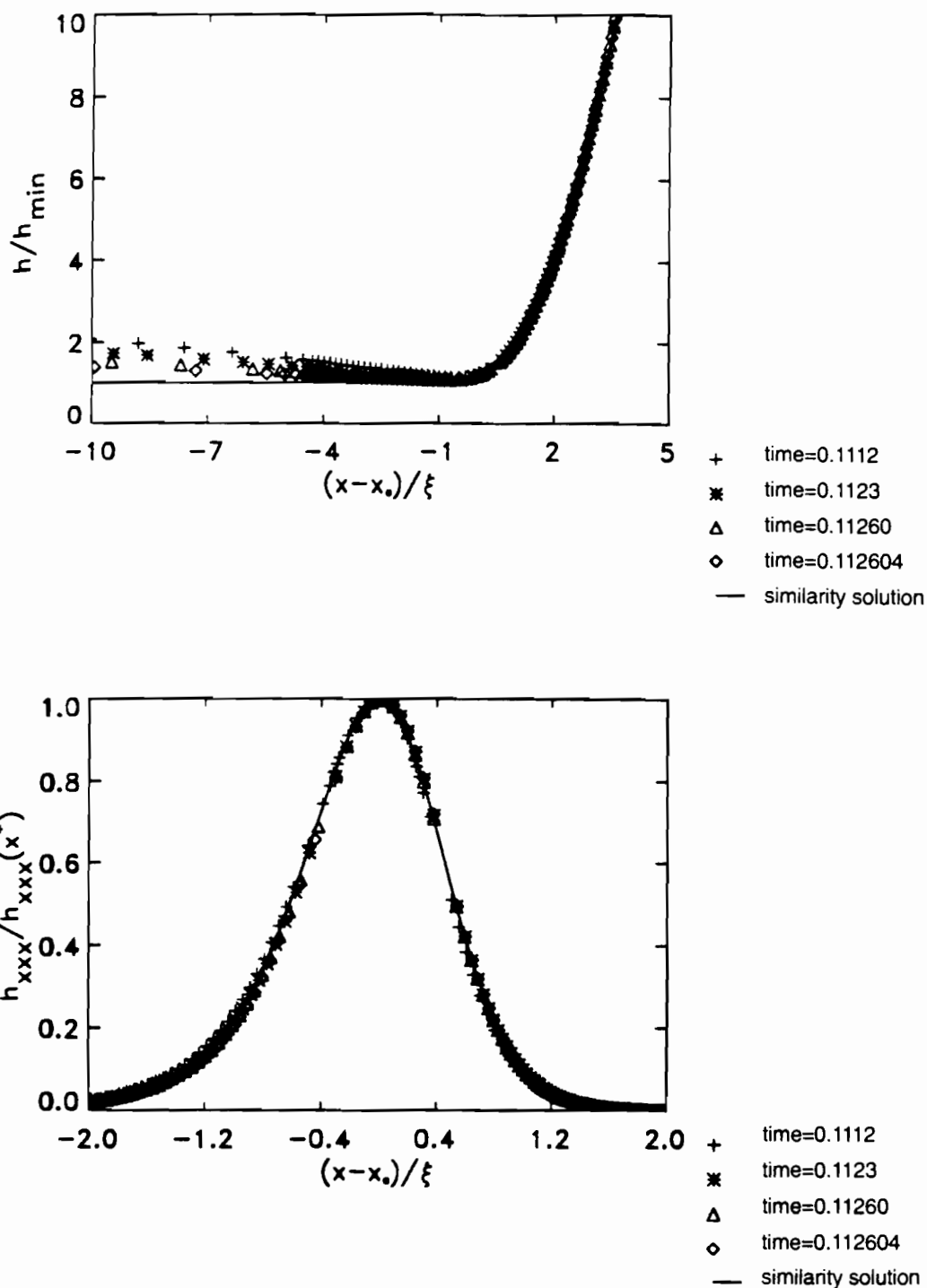△   time=0.11260
◇   time=0.112604
—   similarity solution

FIGURE 3.15. Rescaled profiles near the singularity for $n = 7.5$. The upper figure shows rescaled height profiles, and the lower figure shows rescaled h_{xxx} profiles. Each different symbol represents a numerical solution at a different time. The solid line is a solution to the velocity equation with initial conditions as described in the text. Notice that the scaling breaks down to the right of the minimum.
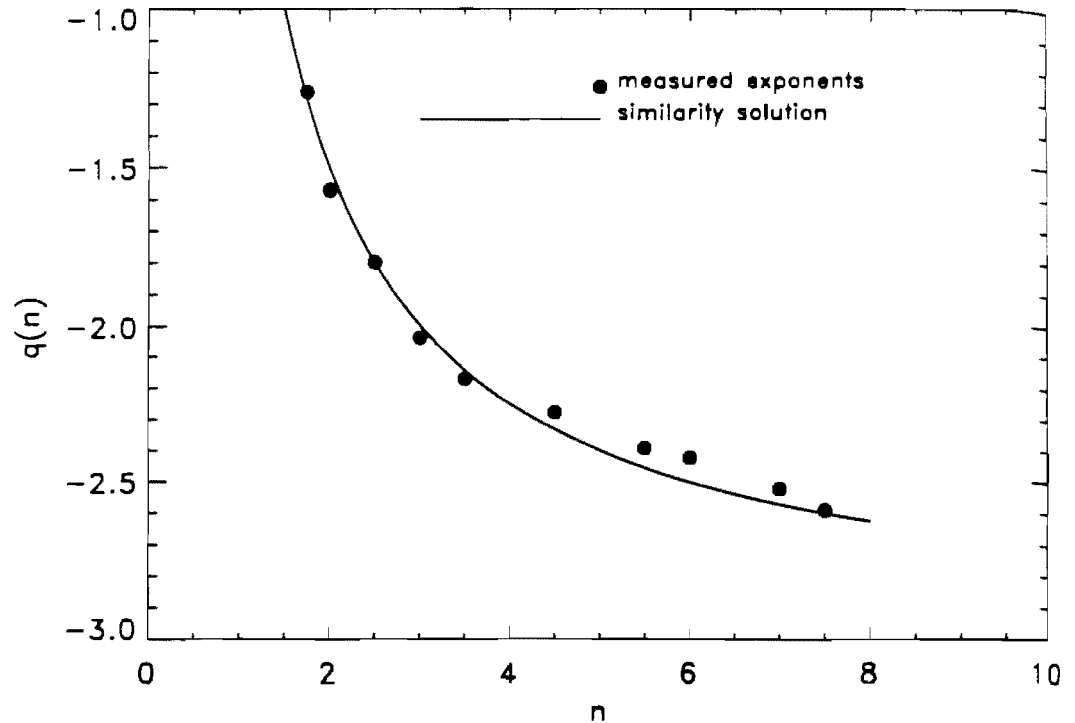
FIGURE 3.16. Exponent $q(n)$ of $h_{xxx}(x^*, t) \sim \xi^{q(n)}$ for boundary singularities with $n \geq 1.5$. The measured exponents are compared with those of the similarity solution.

finite time singularities with symmetric pinch regions for $n < 1$.[5] We also have numerical evidence for these singularities up to $n \approx 1.4$, although at present we have little theory for $n \geq 1$.

For small n ($n < 0.5$) and either "current" or "pressure" boundary conditions with $p > 2$, every initial condition we attempt gives a singularity of this type. For $n > 0.5$, some initial conditions converge to the other singularities discussed above. Typically, this singularity corresponds to choosing $\epsilon \sim 1/64$ and r very small. For each value of n and ϵ there is a critical rate r_c below which solutions generically converge to this type of singularity. For $n = 1$ and $\epsilon = 1/128$, the critical r_c is about 30. The critical rate r_c changes as a function of n.

We construct a similarity solution for these solutions with $n < 1$ as follows: To lowest order, the solution solves the parabolic equation

$$h(x, t) \approx (t_c - t) + Bx^2 \equiv H_0(x, t). \qquad (3.28)$$

---

[5]We note that it is easy to find infinite time singularities with symmetric pinch points; these occur generically when $p = 2$.
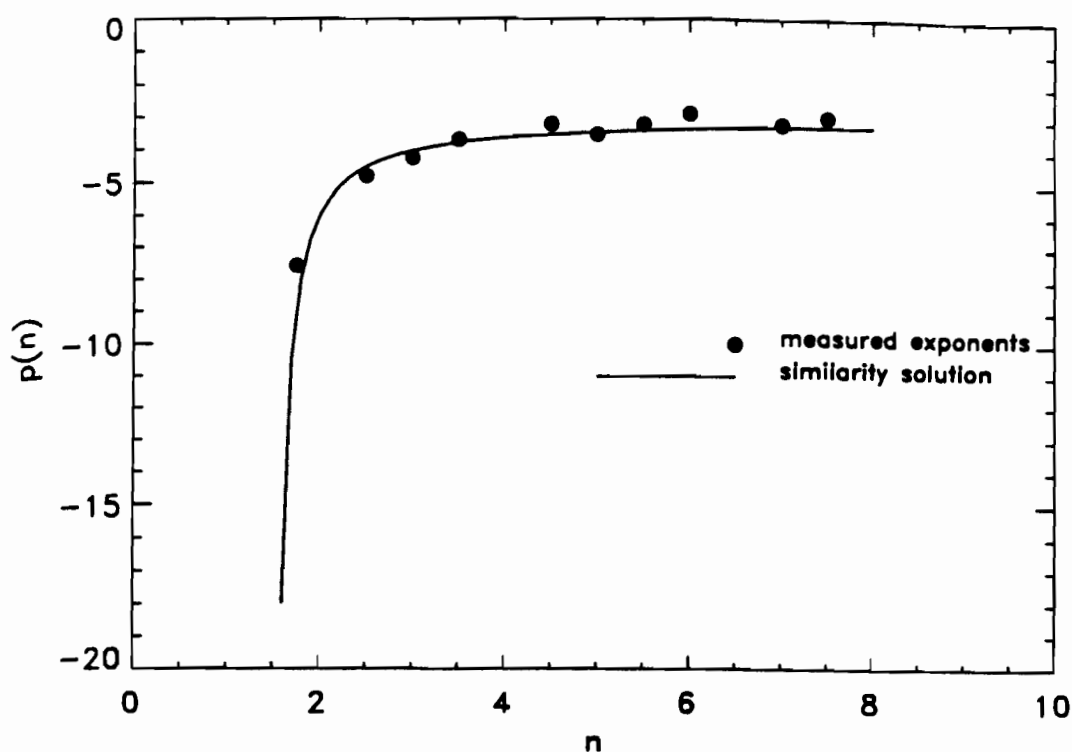
FIGURE 3.17. Exponent $p(n)$ of $h_{xxx}(x^*, t) \sim (t_c - t)^{p(n)}$ for boundary singularities with $n \geq 1.5$. The measured exponents are compared with those of the similarity solution.

Writing $h = H_0 + g$, g must satisfy

comes from rescaling (2.13)

$$((H_0 + g)^n g_{xxx})_x = 1 \qquad (3.29)$$

so that

$$g_{xxx} = \frac{x}{(g + H_0)^n}. \qquad (3.30)$$

We formally expand equation (3.30) in powers of g. If $n < 1$, the successive terms in the expansion decrease for small $|x|$ and $|t_c - t|$.

The first-order correction to H_0 satisfies

$$g_{xxx} = \frac{x}{H_0^n}. \qquad (3.31)$$

In Figure 3.18 we show the dependence of the minimum height, h_{min} on ξ, the characteristic width, for $n = 0.75$. In Figure 3.19 we show the dependence of h_{min} on $t_c - t$ for $n = 0.75$. In both cases, the solid lines represents the prediction of the similarity solution. The agreement is excellent. We also check that the the correction to H_0, which satisfies equation
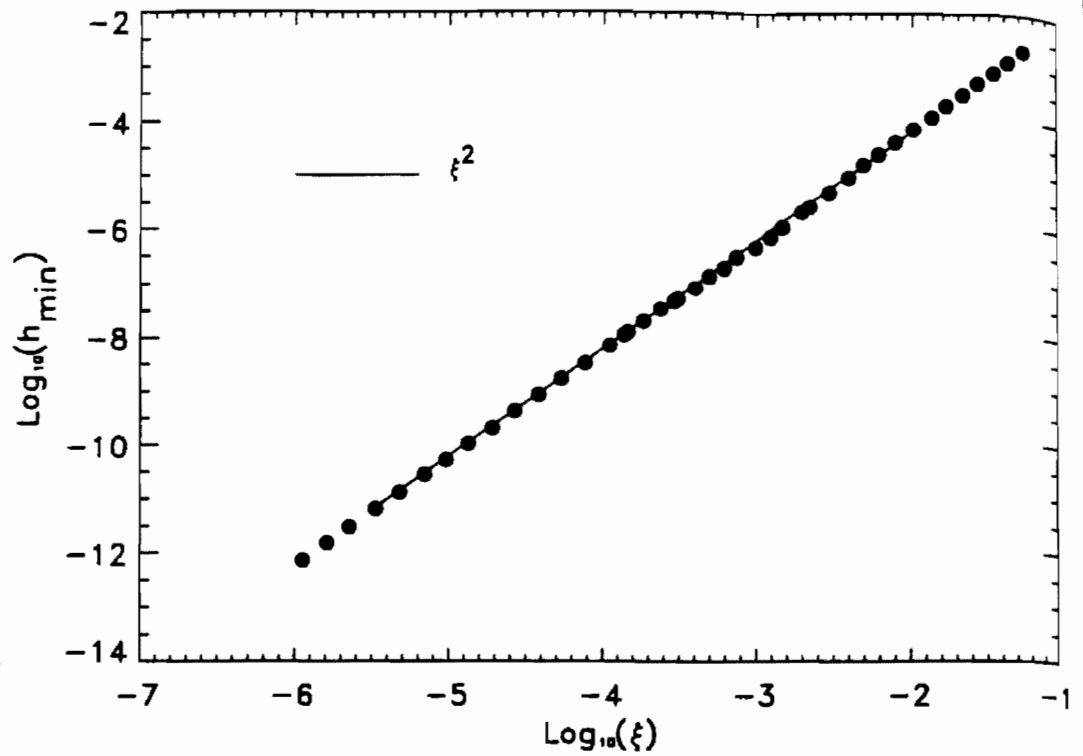
FIGURE 3.18. Dependence of h_{min} on ξ in the pinch region for finite time singularity at $n = 0.75$. We show $\log(h_{min})$ versus $\log(\xi)$. The solid line represents the prediction of the theory.
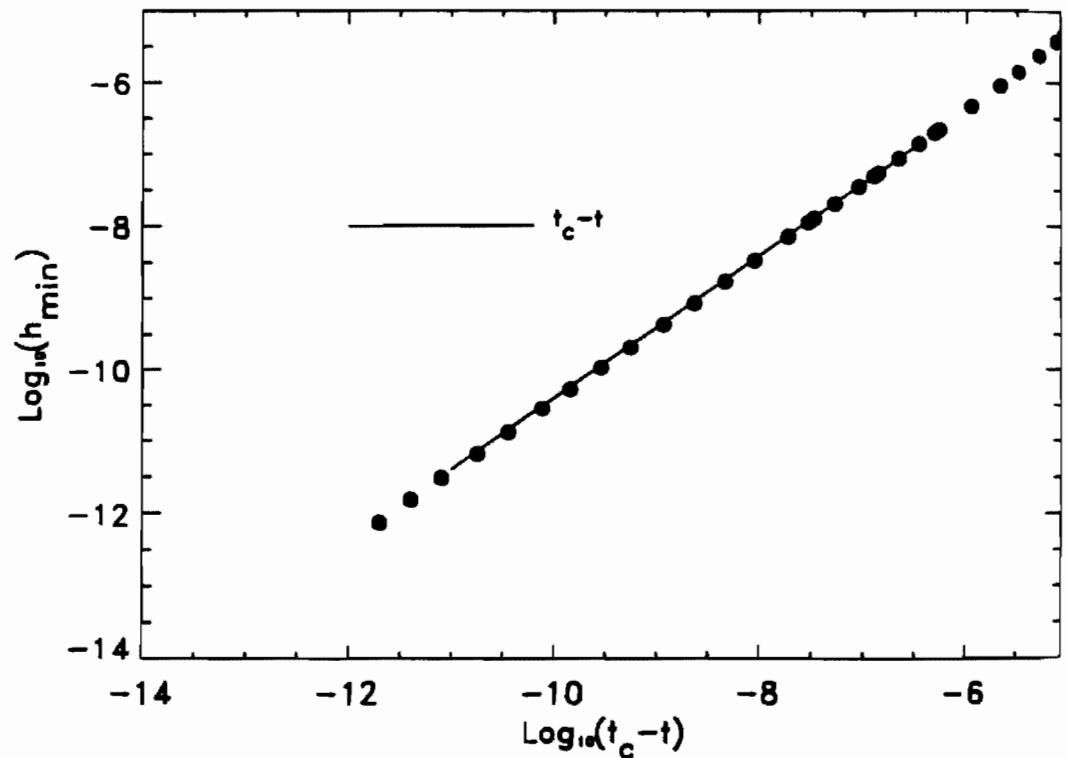

FIGURE 3.19. Time dependences for finite time singularity at $x = 0$ for $n = 0.75$. We show $\log(h_{min})$ versus $\log(t_c - t)$. The solid line represents the prediction of the theory.
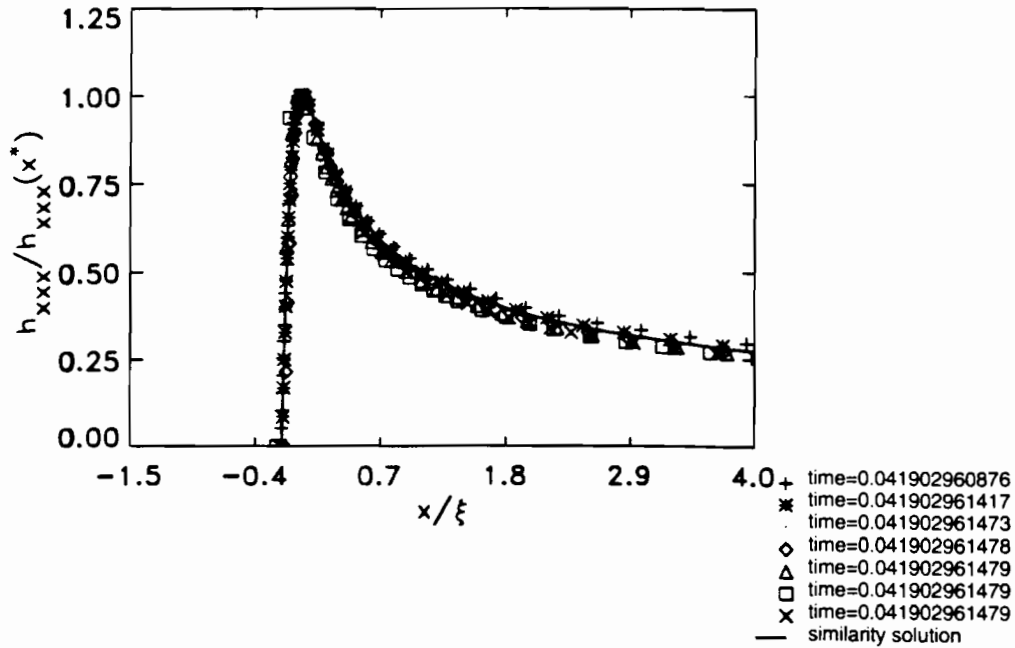
FIGURE 3.20. Rescaled h_{xxx} versus x profiles near the singularity for $n = 0.75$. Each symbol represents a numerical solution at a different time. The solid line is the first-order correction to the parabolic solution, as determined by equation (3.31).

(3.31), is present in the data. We can isolate the correction by examining h_{xxx}. For $n > 0.5$, h_{xxx} has a maximum at

$$x^* = \left(\frac{t_c - t}{B(2n - 1)}\right)^{1/2}. \tag{3.32}$$

In Figure 3.20 we plot $h_{xxx}/h_{xxx}(x^*)$ versus $x/(h_{xxx}(x^*))^{-2}$ for seven different times at $n = 0.75$. The data collapse quite well. The solid line represents a solution (3.31) with $B = 69.2$ In Figure 3.21 we show a similar plot for $n = 0.25$. Here we plot $h_{xxx}(x, t)/h_{min}^{0.25}$ versus $x/h_{min}^{0.5}$ for seven different times. Again the data collapse; the agreement with the similarity solution $B = 2.5$ is excellent. We repeat this analysis for many values of n less than one, with similar agreement. As an example, in Figure 3.22 we show the exponent of $h_{min} \sim \xi^{q(n)}$ as a function of n. The solid line represents the prediction of the similarity solution, and the points are the results of simulations. In Figure 3.23 we show the exponent of $h_{min} \sim (t_c - t)^{p(n)}$ as a function of n, for both theory and simulations. Again the agreement is excellent.
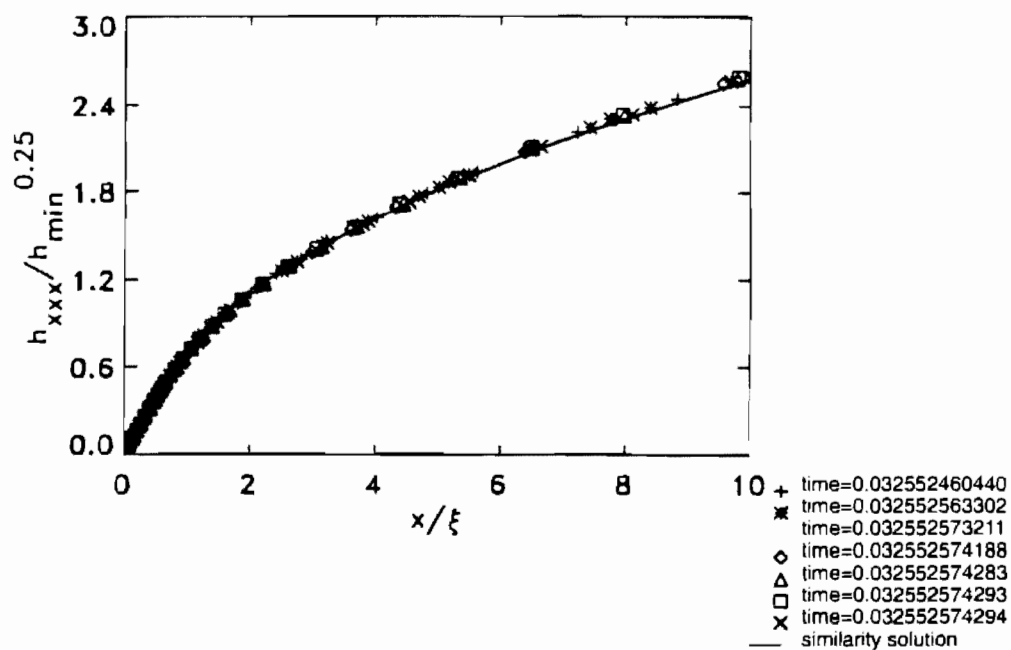
FIGURE 3.21. Rescaled h_{xxx} versus x profiles near the singularity for $n = 0.25$. Each symbol represents a numerical solution for a different time. The solid line is the first-order correction to the parabolic solution, as determined by equation (3.31).
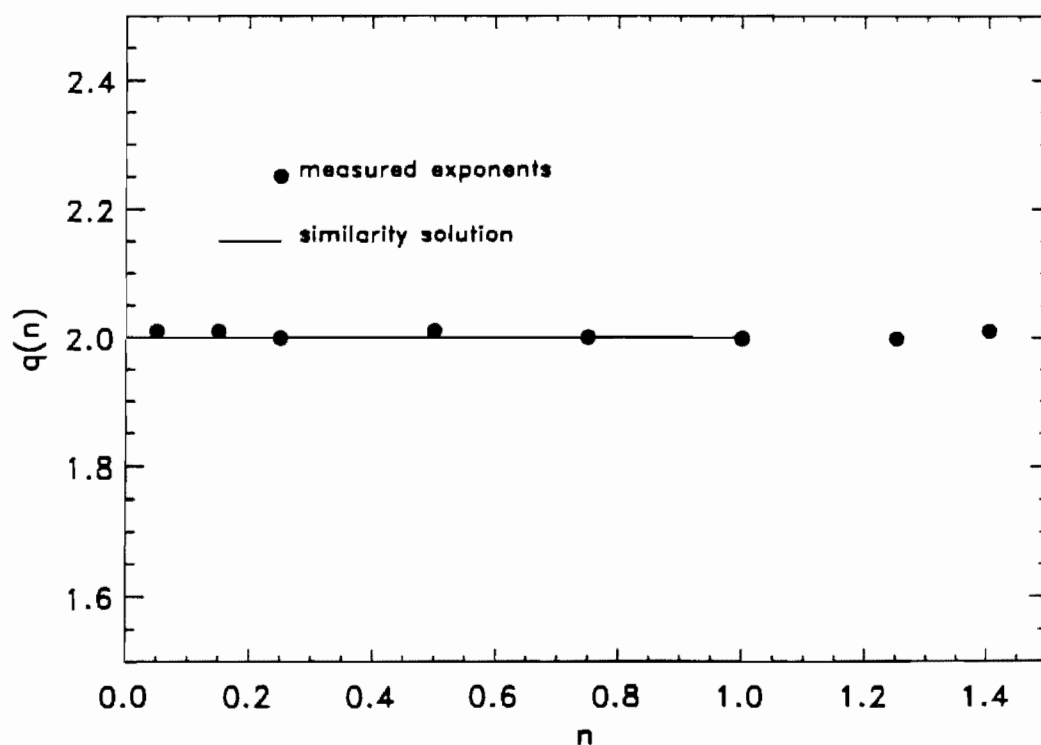

FIGURE 3.22. Exponent $q(n)$ of $h_{min} \sim \xi^{q(n)}$ for finite time touchdown at $x = 0$. The measured values are compared with the exponents of the similarity solution.
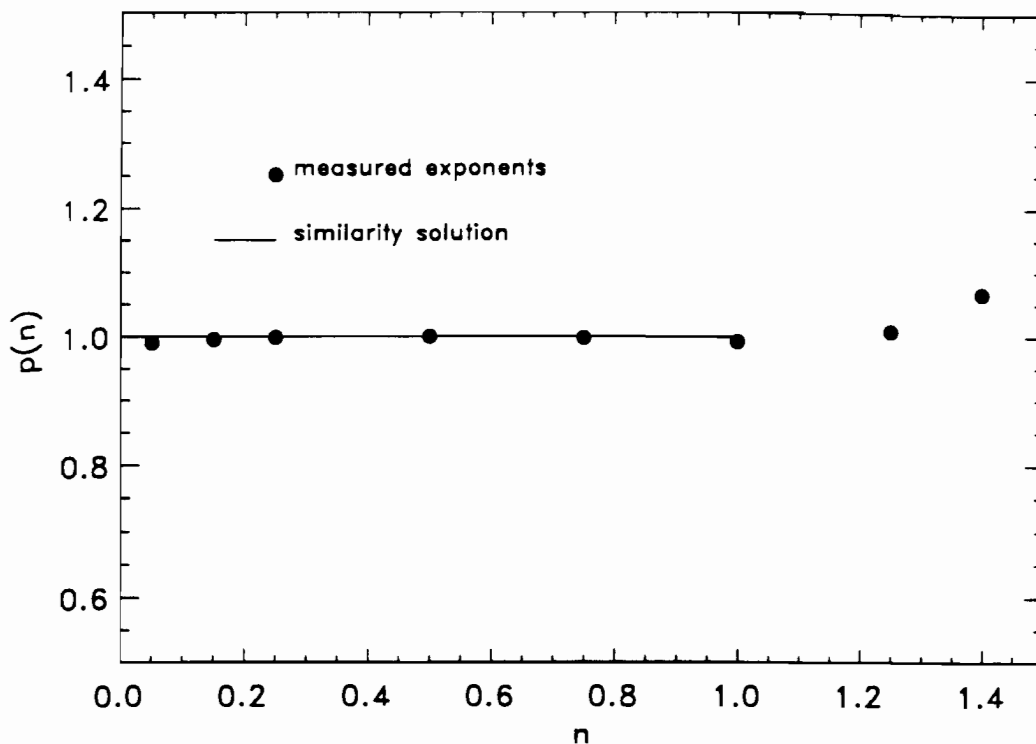
FIGURE 3.23. Exponent $p(n)$ of $h_{min} \sim (t_c - t)^{p(n)}$ for finite time touchdown at $x = 0$. The measured values are compared with the exponents of the similarity solution.

We also include in Figure 3.22 and 3.23 points for $n > 1$. Although it is possible (with a slight modification) to construct a similar expansion for $1 \leq n < 2$, such solutions do not agree with the measured exponents. Numerically we do not seem to observe this singularity all the way up to $n = 2$.

6.4   Unsolved Problems

6.4.1   Singularities and Similarity Solutions

In Section 6.3, we describe many singularities of the model equation (1.11) which exhibit self-similar structure. We compare the characteristics of these singularities to those of various similarity solutions that approximate the model equation. Our analysis is in the spirit of matched asymptotics, formulated for analyzing the solutions of ordinary differential equations [12]. In order for a similarity solution to describe the region around the singularity (the inner region) we must be able to match the solution to boundary

2552460440
2552563302
2552573211
2552574188
2552574283
2552574293
2552574294
solution

or $n = 0.25$.
e solid line
by equation

1.4
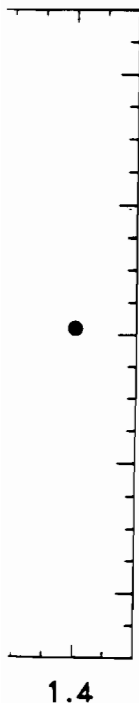
n at $x = 0$.
ty solution.

conditions (the outer region). We discover in Section 6.3 that in many in-stances, the matching is sufficient to qualitatively predict transitions in the model PDE. The transitions obtained via the matching principle are con-sistent with the transitions observed in the numerical solutions. However, matching conditions for PDEs are much more complicated than those in traditional problems of matched asymptotics; in particular, we must in-clude the time dependence of the solutions. We are completely successful in only two cases: the infinite time singularities and the finite time singular-ities at $x = 0$, for $n < 1$. These cases both have "singular" minimum points that do not propagate. In the cases where the singular points do propagate, that of edge singularities and finite time singularities at $0 < x_0 < 1$, we do not have a complete matching analysis. In both of these cases, we have a consistent theory for the leading order behavior of the singularity but we do not know how to match this behavior to the rest of the solution. A third case with incomplete analysis is that of finite time singularities at $x_0 = 0$ for $n \geq 1$.

The construction of a singular solution using matched asymptotics is im-portant because it indicates that the numerical solution reflects properties of the PDE. Whether this solution is actually realized in practice depends on its stability. Brenner and Bertozzi [6] proved linear stability for a two-dimensional variant of the $q = -1$ solution. Their analysis also shows that the $q = -1$ solution and the parabolic solution of Section 6.3.2 are linearly stable to perturbations with support inside the support of the similarity solution. Our simulations indicate that many other similarity solutions are stable, although at present we have no proof.

In the cases where there is not a similarity solution we exercise extreme caution when interpreting numerical results on singularity formation. We must keep in mind that the simulations only track the solutions to a mini-mum height, typically $10^{-15} - 10^{-20}$. We cannot rule of the possibility that the numerical solutions do not converge on a particular self-similar singu-larity uniformly as $h \to 0$; instead a completely different type of behavior could set in at a small height beyond our resolution. When a similarity solution exists, we know that the numerical singularity is a true singularity of the PDE. However, in cases where there is no theory, simulations alone do *not* provide ample evidence for the existence of a singularity. As an in-dication of the subtlety of this issue, we describe a situation that arises for $n = 1.6$, with initial conditions described in Section 6.3.1. The solu-tion initially appears to be the same type of singularity as the finite time singularities at $x = 0$. However, when the minimum height reaches below 10^{-15}, the nature of the solution changes drastically. The minimum be-gins to propagate toward the boundary, carrying with it an extraordinarily complicated structure. Figure 4.1 shows height profiles of the singularity at early times, and Figure 4.2 shows height profiles at slightly later times. Without rigorous theory to support the data, we can never be certain that the equation will not "fool" us in this way.

many in-
ons in the
e are con-
However,
n those in
· must in-
successful
e singular-
um points
propagate,
< 1, we do
we have a
ty but we
n. A third
at $x_0 = 0$

tics is im-
properties
e depends
for a two-
hows that
re linearly
similarity
utions are

e extreme
ation. We
to a mini-
bility that
lar singu-
behavior
similarity
ingularity
ions alone
As an in-
hat arises
The solu-
inite time
hes below
imum be-
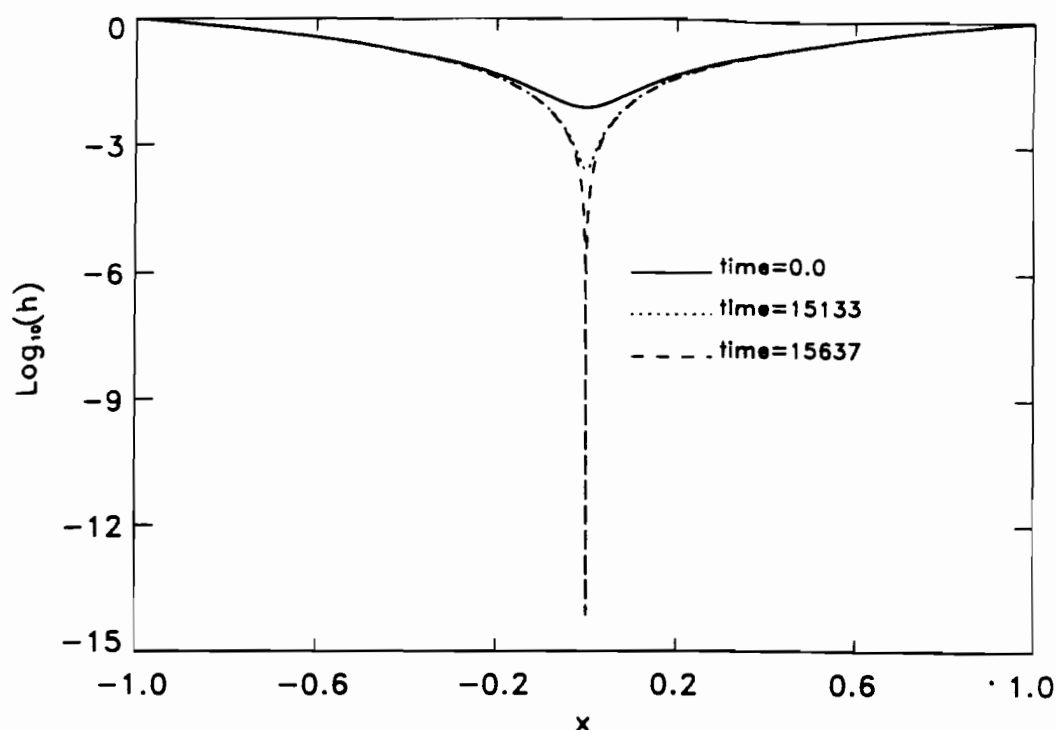ordinarily
ingularity
ter times.
rtain that

FIGURE 4.1. Early time structure of solution for $n = 1.6$. It appears that there will be a singularity at $x = 0$.

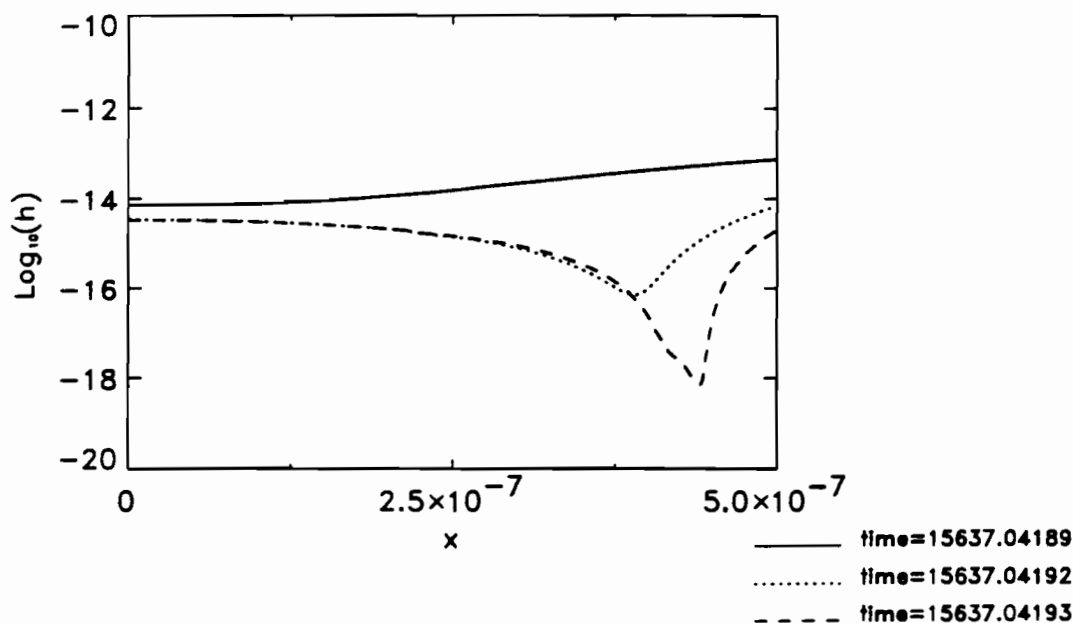FIGURE 4.2. Blow-up of the preceding $n = 1.6$ solution at a slightly later time. The minimum is no longer at $x = 0$.
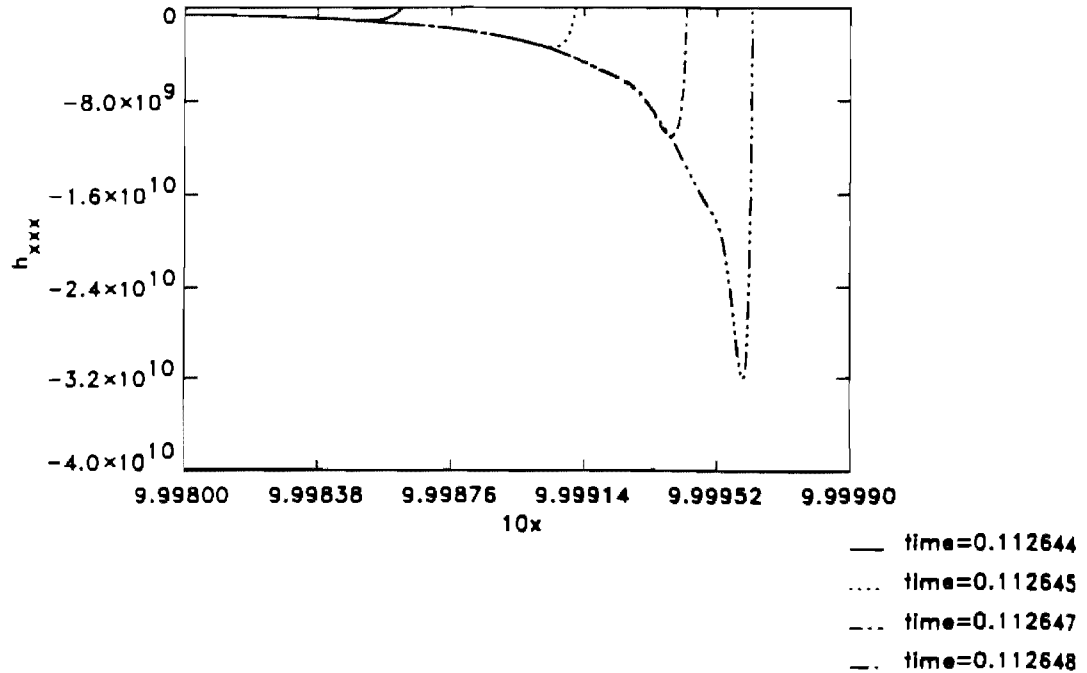
0

-8.0×10^9

-1.6×10^{10}

h_{xxx}

-2.4×10^{10}

-3.2×10^{10}

-4.0×10^{10}

9.99800   9.99838   9.99876   9.99914   9.99952   9.99990

10x

—— time=0.112644

.... time=0.112645

_... time=0.112647

_. time=0.112648

FIGURE 4.3. Numerical solutions at the foot of the maximum of the h_{xxx} profile in the case of edge singularity for $n = 7.5$.

6.4.2 Complex Singularities

This chapter focuses on similarity solutions which are extremely prevalent in the data. However, not all of the observed singularities are self-similar. As an illustration of the complex behavior, we discuss two examples: The first arises near the minimum of h in the edge singularity. As we discuss in Section 6.3, the similarity solution does not account for the small flux traveling across the pinch region from the central region. This flux causes an interesting dynamic structure near the minimum of h. Figure 4.3 shows the typical behavior we observe for higher values of n. It depicts successive profiles of h_{xxx} versus x, to the left of the minimum for $n = 7.5$. (Recall that the theory of Section 6.3 applies only to the right of the minimum.) We see the formation of a pronounced "dip," which has scaling structure with *different* exponents than the scaling theory presented in Section 6.3. This singularity thus has two different scaling regions. Values of n closer to the critical value 1.5 produce solutions which have an even more complex structure. Figure 4.4 shows the analogous profiles for $n = 2.5$. As in the $n = 7.5$ case, a "dip" begins to form. However, as depicted in Figure 4.5, at later times the profile has irregular oscillations with a frequency that increases as $t \to t_c$. We greatly resolve these oscillations to ensure that they are not produced by the numerics.

>ff

$$\text{--- time=0.1476}$$
$$\text{.... time=0.1525}$$
$$\text{-.. time=0.1570}$$

me=0.112644

me=0.112645

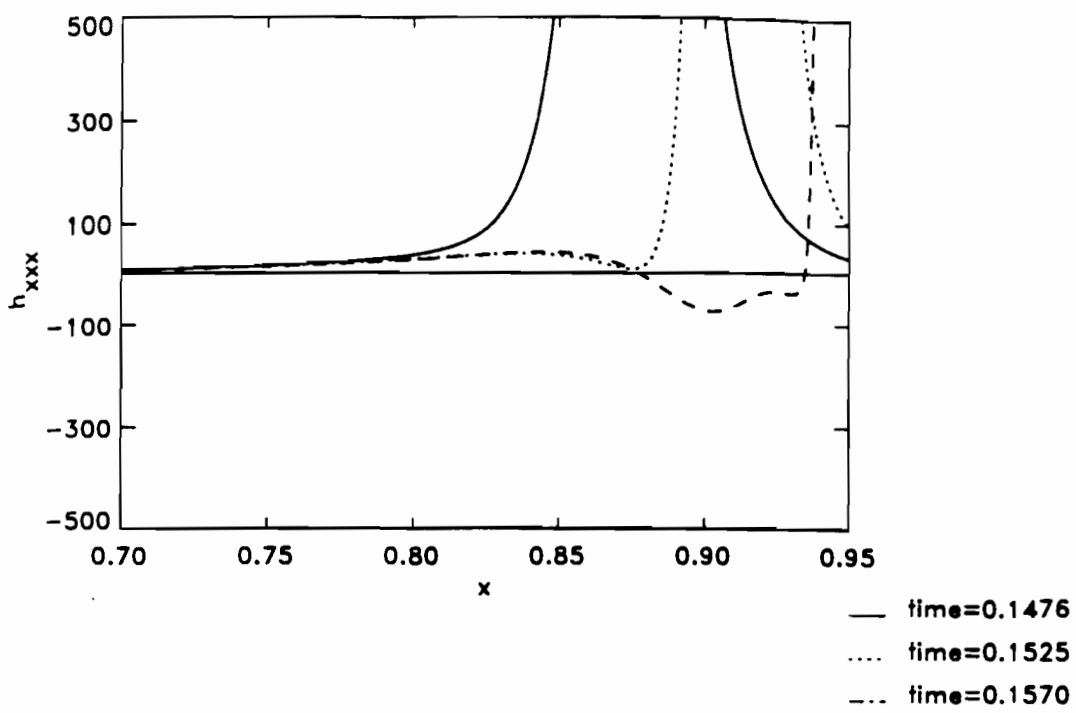me=0.112647

me=0.112648

h_{xxx} profile

FIGURE 4.4. Numerical solution at the foot of the maximum of the h_{xxx} profile in the case of edge singularity for $n = 2.5$. Note the formation of a foot-like structure, as in the $n = 7.5$ case.
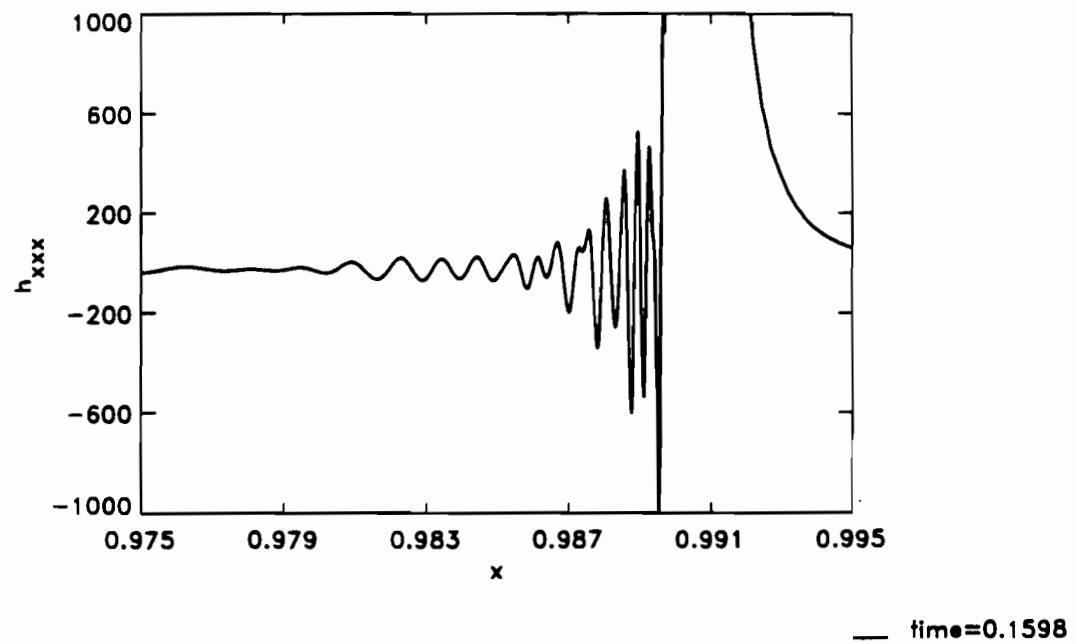
prevalent
elf-similar.
nples: The
we discuss
small flux
lux causes
4.3 shows
successive
.5. (Recall
ninimum.)
; structure
ection 6.3.
n closer to
e complex
As in the
igure 4.5,
iency that
isure that

$$\text{--- time=0.1598}$$

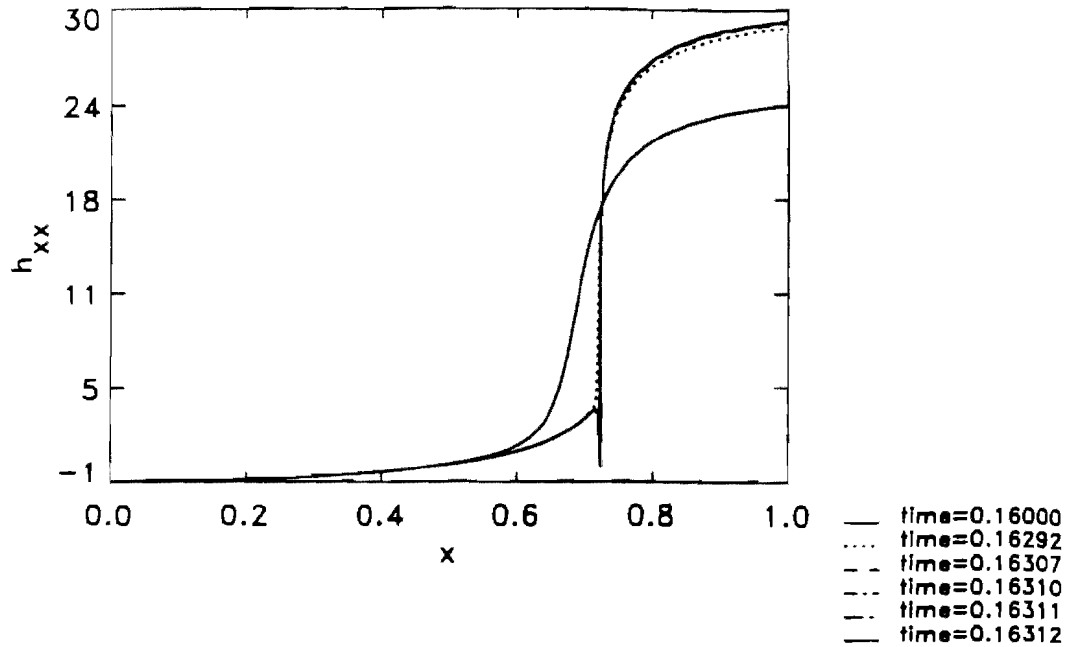FIGURE 4.5. Numerical solution near the foot for $n = 2.5$ at a later time.

FIGURE 4.6. Successive time profiles of h_{xx} versus x for $n = 1.4$ with pumping boundary conditions. The gross feature of the plot is that as the singularity is reached, the profile is mainly monotonic with a pronounced tip that was not present for the cases $0.75 < n < 1.25$.

Another complex singularity arises generically for current boundary conditions with $1.5 > n > 1.25$. In the previous section, we argue that in the pinch region simulations with $0.75 \leq n \leq 1.25$ the current equation represents the leading order behavior for these solutions. This solution has the feature that h_{xx} is monotonic in x in the pinch region. In contrast, Figure 4.6 shows successive time profiles of h_{xx} versus x for $n = 1.4$. Here, although the global picture looks somewhat monotonic, it is actually considerably more complicated. To see this, in Figure 4.7 we blow up the area around the pinch which contains a local minimum in h_{xx} in the shape of a "tip." Blowing up the "tip" region again in Figure 4.8 we see that this is not a simple minimum, but in fact it posseses another tip, which, in turn, has yet another tip upon finer resolution. We do not know whether this type of structure persists until the singularity.

6.4.3   Mathematical Questions

A number of important mathematical questions still remain. For instance, what is the critical value of n, above which finite time singularities are impossible? Is it the same for all boundary conditions? The theorems of
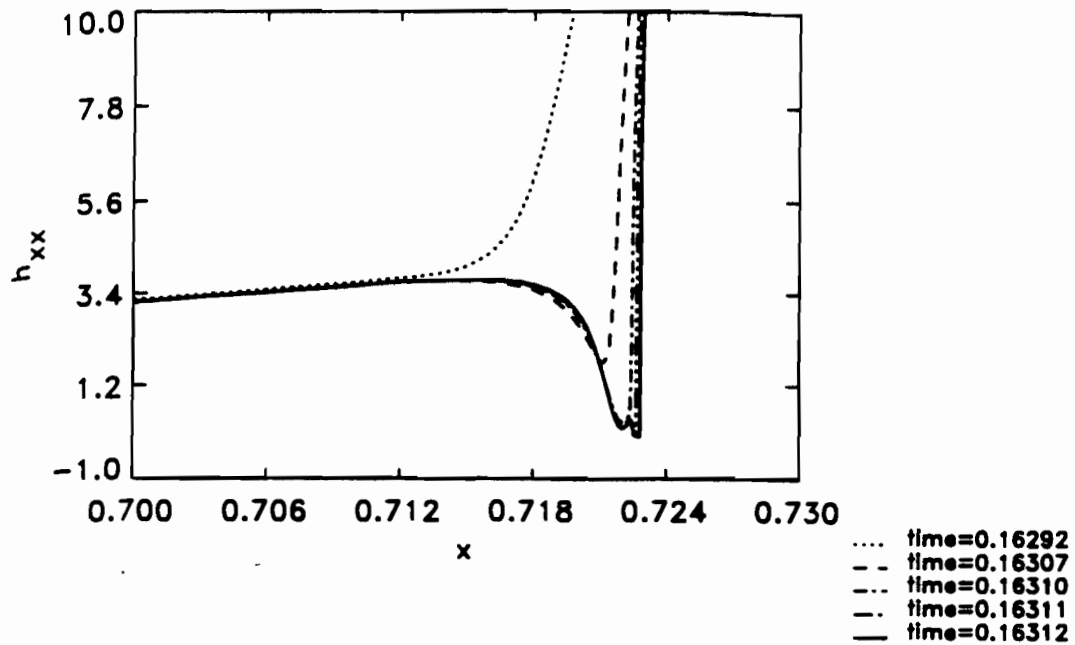
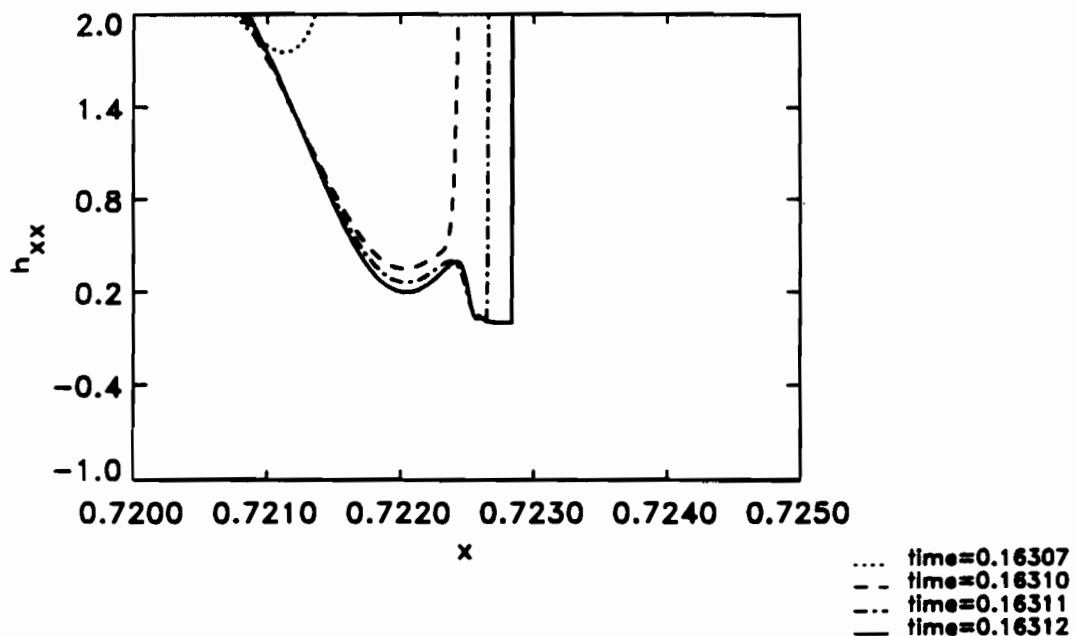FIGURE 4.7. Blow-up of the previous figure. Notice the "tip" has the added structure of a smaller tip.

FIGURE 4.8. Blow-up of the "tip" region in the previous figure. The "tip" region also has a "tip".

Section 6.1 place an upper bound on this critical value of n. However, our simulations indicate that the critical value is probably lower. Another open problem is a rigorous proof for the existence of finite time singularities at *any* nonzero value of n larger than zero. Our numerical simulations are convincing evidence for the possibility of such a proof. A related problem not addressed in this chapter is the continuation of solutions beyond the singularity. Bernis and Friedman [3] prove the global in time existence of non-negative weak solutions for $n \geq 1$ with the boundary conditions (1.14). However, uniqueness is unknown. An open problem is whether or not additional boundary conditions (on the edge of the support of the solution) are needed after the singularity. If such conditions are needed, how do we pick out the physically relevant solutions? Perhaps similarity solutions again play a role, as in the work of Keller and Miksis describing a related but different surface tension problem [21].

Another issue not discussed in this chapter is comparison with experiment. The only practically realizable systems correspond to $n = 1$ (Hele–Shaw cell) and $n = 3$ (thin film on solid surface). There is reason to believe that our singularity results apply to Hele–Shaw experiments with sufficiently viscous fluids (see [4]). Experiments on singularities in Hele–Shaw systems are in progress (see [16, 18]). Hopefully the results will stimulate further theoretical developments.

References

[1] G.K. Batchelor, *An Introduction to Fluid Dynamics*. Cambridge University Press, Cambridge, 1967.

[2] D. Bensimon, L.P. Kadanoff, S. Liang, B.I. Schraiman, and C. Tang, Viscous flows in two dimensions. *Rev. Mod. Phys.* **58**, 977 (1986).

[3] F. Bernis and A. Friedman, Higher order nonlinear degenerate parabolic equations. *J. Diff. Equations* **83**, 179–206 (1990).

[4] A. Bertozzi, M. Brenner, T. Dupont, and L. Kadanoff. Unpublished results.

ınoff

However, our
Another open
ngularities at
mulations are
ated problem
s beyond the
me existence
y conditions
s whether or
pport of the
are needed,
ps similarity
is describing

with experi-
ı = 1 (Hele–
on to believe
s with suffi-
ı Hele–Shaw
ill stimulate

partment of
University of
ly supported
upport of a
wing people
tantin, Ray
grateful to

ıbridge Uni-

ad C. Tang,
7 (1986).

ıerate para-

Inpublished

[5] Stephanella Boatto, Leo Kadanoff, and Piero Olla, *Phys. Rev. E* **48**, 4423 (1993).

[6] M. Brenner and A. Bertozzi, On the spreading of droplets on a solid surface. *Phys. Rev. Lett.* **71**(4), 593–596 (1993).

[7] A. Cameron, *Principles of Lubrication*. Longmans, London, 1966.

[8] P. Constantin, T. Dupont, R. Goldstein, L. Kadanoff, M. Shelley, and S. Zhou, Droplet breakup in a model of the Hele–Shaw cell. *Phys. Rev. E* **47**(6), 4169–4181 (1993).

[9] P.G. de Gennes, Wetting: Statics and dynamics. *Rev. Mod. Phys.* **57**, 827–863 (1985).

[10] C. Domb and M.S. Green (eds.), *Phase Transitions and Critical Phenomena*. Academic Press, London, 1972.

[11] T. Dupont, R. Goldstein, L. Kadanoff, and S. Zhou, Finite-time singularity formation in Hele–Shaw systems. *Phys. Rev E* **47**(6), 4182–4196 (1993).

[12] M. Van Dyke, *Perturbation Methods in Fluid Mechanics*. Parabolic Press, Stanford, CA, 1975.

[13] J. Eggers and T.F. Dupont, Drop formation in a one-dimensional approximation of the Navier–Stokes equation. To appear, *J. Fluid Mech.*

[14] M.J. Shelley, R.E. Goldstein, and A.I. Pesci, Topological transitions in Hele–Shaw flow. In *Singularities in Fluids, Plasma, and Optics*, R.E. Caflisch and G.C. Papanicolou (eds.), pp. 167–188.

[15] R.E. Goldstein, A.I. Pesci, and M.J. Shelley, Topology transitions and singularities in viscous flows. *Phys. Rev. Lett.* **70**(20), 3043–3046 (1993).

[16] R.E. Goldstein, T.G. Mason, and E. Shyamsunder. Private communication.

[17] H.P. Greenspan, On the motion of a small viscous droplet that wets a surface. *J. Fluid Mech.* **84**, 125–143 (1978).

[18] D. Grier and N. Morgan. Private communication.

[19] L.M. Hocking, Sliding and spreading of this two-dimensional drops. *Quart. J. Mech. Appl. Math.* **34**, 37–55 (1981).

[20] Chun Huh and L.E. Scriven, Hydrodynamic model of steady movement of a solid/liquid/fluid contact line. *J. Colloid Interface Sci.* **35**, 85–101 (1971).

[21] J.B. Keller and M.J. Miksis, Surface tension driven flows. *SIAM J. Appl. Math.* **43**(2), 268–277 (1983).

[22] R.M. Kerr, Evidence for a singularity of the three dimensional incompressible Euler equations. *Phys. Fluids A* **5**, 1725 (1993).

[23] A.J. Majda, Vorticity and the mathematical theory of incompressible fluid flow. *Comm. Pure Appl. Math.* **39**, 5187–5220 (1986).

[24] P. Neogi and C.A. Miller, *J. Colloid Interface Sci.* **92**, 338 (1984).

[25] A. Pumir and E.D. Siggia, Development of singular solutions to the axisymmetric Euler equations. *Phys. Rev. Lett.* **68**, 1511–1514 (1992).

[26] E.B. Dussan V and S. Davis, On the motion of a fluid-fluid interface along a solid surface. *J. Fluid Mech.* **65**, 71–95 (1974).

[27] Robert M. Wald, *General Relativity*. University of Chicago Press, Chicago, 1984.

[28] S. Zhou, *Interface Dynamics: Bubble Growth and Droplet Breakup in the Hele-Shaw Cell*. Ph.D. thesis, University of Chicago, 1992.

ARMA 128(2) 165-205